https://doi.org/10.5194/egusphere-2026-6213
Preprint. Discussion started: 26 November 2026
© Author(s) 2026. CC BY 4.0 License.

Impact of glacio-isostasy on topography, hydrology and drainage patterns in the southern North Sea

Ruben Bertels[1,2] & Marc De Batist[2]

[1] Department of Physical Geography and Geoecology, Charles University, Prague, Czechia
[2] Renard Centre of Marine Geology, Department of Geology, Ghent University, Ghent, Belgium

Correspondence to: Ruben Bertels (ruben.bertels@natur.cuni.cz)

https://doi.org/10.5194/egusphere-2026-6213
Preprint. Discussion started: 26 November 2026
© Author(s) 2026. CC BY 4.0 License.



ABSTRACT

During the Last Glacial Period, the North Sea was bordered by the British-Irish Ice Sheet (BIIS) and the Fennoscandian Ice Sheet (FIS), which coalesced over the exposed basin during periods of maximal ice-sheet expansion. Sedimentological evidence indicates that a proglacial lake may have existed south of the ice margin, although there is still large uncertainty about their exact extent and volume, partly because most reconstructions have largely neglected glacio-isostatic deformation as a contributing factor. We quantified glacio-isostatic deformation of the North Sea basin between 80 and 15 ka using two published ice-sheet reconstructions as forcing in a glacio-isostatic adjustment model that accounts for lithospheric flexure and asthenospheric viscous response. Our results show that during peak glacial phases, particularly Marine Isotope Stages (MIS) 2 and 4, the region south of the ice margin subsided by as much as 100 m. Combined with the low-relief topography of the Oyster Ground region, this deformation created sufficient accommodation space for a proglacial lake with a volume of up to 3000 km³. Following separation of the BIIS and FIS, the lake likely drained northward, potentially as a glacial lake outburst flood. Beyond the area affected by subsidence, glacio-isostatic adjustment generated a flexural forebulge, with maximum uplift beneath the present-day Netherlands, which may have contributed to the southward displacement of the Rhine during MIS 3. These results demonstrate that glacio-isostatic deformation is a key control on the evolution of proglacial lakes and drainage pathways in formerly glaciated basins.

https://doi.org/10.5194/egusphere-2026-6213
Preprint. Discussion started: 26 November 2026
© Author(s) 2026. CC BY 4.0 License.

1. INTRODUCTION

The growth of continental ice sheets during glaciation significantly influences landscape evolution by lowering global sea level through large-scale storage of ocean water on land. During the Last Glacial Maximum (LGM), for instance, eustatic sea level was ca. 120-135 m below present (Clark and Mix, 2002). Ice loading itself also modifies topography via glacial isostatic adjustment (GIA), whereby the weight of the ice depresses the lithosphere into the asthenosphere, while generating an uplifted forebulge or peripheral bulge beyond the ice margins (Whitehouse, 2018). Because GIA operates at millennial timescales, the adjustment of the Earth system to ice loading and loss is a slow process that lags thousands of years behind the actual ice volume changes (Schumacher et al., 2018): i.e., regions that were glaciated during the LGM are presently still uplifting, while peripheral bulges, such as the North Sea forebulge associated with the European ice sheets, still continue to subside (Kiden et al., 2002). By controlling relative sea-level change and shoreline migration (Lambeck, 1995), GIA exerts a major influence on glaciological, geomorphological and sedimentological processes. Quantifying present-day GIA is therefore essential for robust assessments of future sea-level rise under anthropogenic global warming.

The southern North Sea basin has been repeatedly reshaped by the Quaternary glaciations. During the last three of these glaciations –the Elsterian, Saalian and Weichselian– the British-Irish and Scandinavian/Fennoscandian ice sheets (BIIS and FIS, respectively) expanded and coalesced across the central North Sea. The formation of ice-dammed proglacial lakes to the south of the ice margin has been proposed for these glacial periods (e.g., Gibbard, 2007, 1995; Gibbard and Cohen, 2015; Murton and Murton, 2012; Hjelstuen et al., 2018; Patton et al., 2017). However, their exact extent and volume remain uncertain, partly because most reconstructions did not fully account for the effect of GIA. Further away from the ice margin, GIA also influenced landscape development in the southern North Sea. Peripheral forebulge uplift, for example, has been linked to valley incision and river deflection during both the last glacial period (Busschers et al., 2007) and the penultimate glaciation (De Clercq et al., 2018).

Here, we reconstruct GIA-related subsidence and uplift in the southern North Sea resulting from loading by the BIIS and FIS. Owing to limited constraints on the extent and thickness of the Eurasian ice sheets prior to the last glaciation, and to minimal ice present during MIS (marine isotope stage) 5, our simulations commence at MIS 4, span MIS 3-2, and terminate at Termination I. The results provide a framework to evaluate GIA impacts on regional relief, landscape evolution and drainage development south of the ice margin. Specifically, we test whether glacio-isostatic subsidence created accommodation space for proglacial lakes, whether forebulge uplift formed a topographic barrier that helped confine these lakes, and whether zones of maximum uplift were capable of modifying river courses. Where supported, we quantify the timing, duration, and magnitude of vertical displacement, not with the intention to propose these quantifications as definitive or absolute constraints, but rather as plausible end-member scenarios for testing geomorphological and geological interpretations.

The calculations employ two ice-sheet reconstructions as input to a simplified yet robust GIA model that represents the Earth as an elastic lithosphere overlying a viscoelastic asthenosphere. Sensitivity analyses

https://doi.org/10.5194/egusphere-2026-6213
Preprint. Discussion started: 26 November 2026
© Author(s) 2026. CC BY 4.0 License.

explore plausible ranges of Earth parameters, allowing assessment of parameter influence and model robustness.

2. GEOLOGICAL AND ENVIRONMENTAL SETTING

The North Sea is a shallow, epicontinental marginal sea on the northwestern European continental shelf, located between the British Isles and mainland Europe. It has been strongly affected by the Quaternary glaciations, with evidence of at least three major glaciations during the past ca. 0.5 Myr, when both the BIIS and FIS advanced and even coalesced across the central North Sea, i.e., during the Elsterian (MIS 12), the Saalian (MIS 10-6) and the Weichselian (MIS 5d-2) (Fig. 1). Sedimentary records have revealed even older glacial imprints within the basin and have shown distinct differences in regional extent of the ice sheets during these three glaciations, with ice sheets advancing further south on the British side of the North Sea during the Elsterian and Weichselian, while during the Saalian the maximum southward extension occurred on the eastern side of the North Sea (Graham et al., 2011; Eaton et al., 2020).

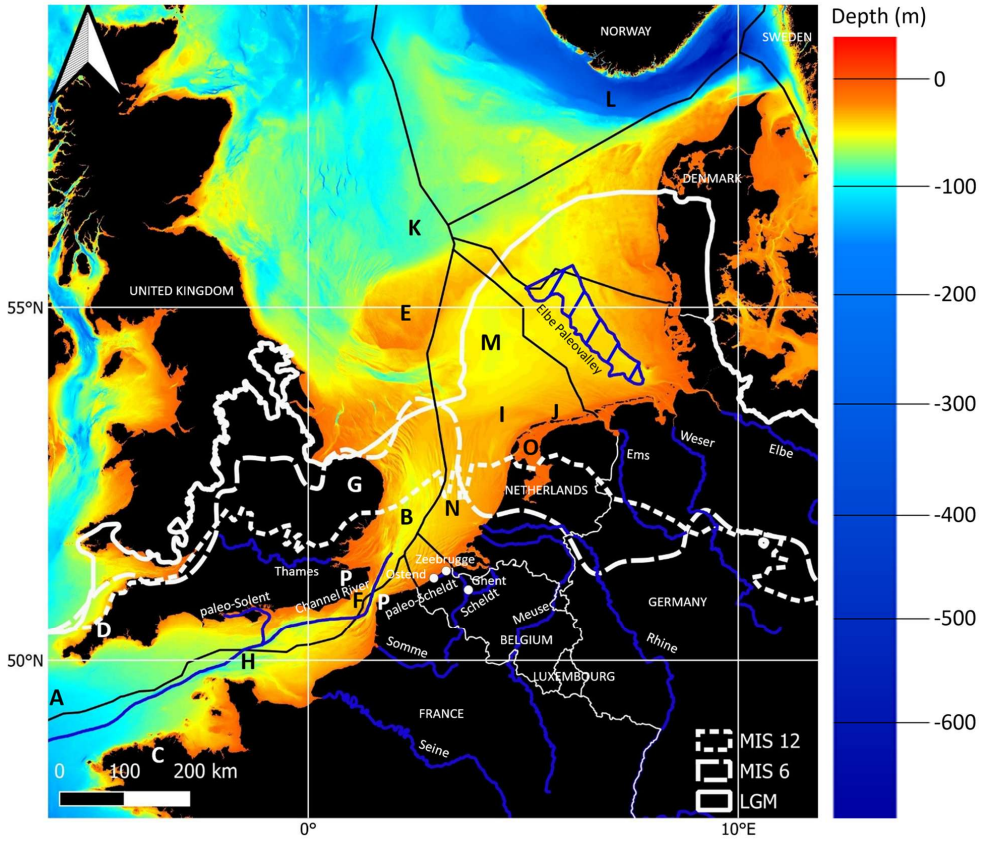

https://doi.org/10.5194/egusphere-2026-6213
Preprint. Discussion started: 26 November 2026
© Author(s) 2026. CC BY 4.0 License.

Figure 1: Bathymetry of the North Sea Basin. Data derived from EMODnet Map Viewer: https://emodnet.ec.europa.eu/geoviewer/. MIS 12, MIS 6 and LGM ice limits are best estimates from Batchelor et al. (2019). Course of the paleo-Solent is after Westaway et al. (2006), course of the paleo-Scheldt is after De Clercq et al. (2018) and location of the Elbe Paleovalley is after Özmaral et al. (2022). A = Atlantic Ocean; B = Axial Channel; C = Brittany; D = Cornwall; E = Dogger Bank; F = Dover Strait; G = East Anglia; H = English Channel; I = Frisian Front; J = Frisian Islands; K = North Sea; L = Norwegian Channel; M = Oyster Ground; N = Southern Bight; O = Wadden Sea; P = Weald-Artois anticline.

During large parts of these glacial periods, the southern North Sea was emergent and hosted a terrestrial environment. Glaciolacustrine deposits preserved onshore in East Anglia and the Netherlands, as well as offshore around Dogger Bank suggest the existence of small- to medium-sized proglacial lakes, dammed by moraines and fed by meltwater during ice retreat (e.g. Cameron et al., 1992; Cotterill et al., 2017). The existence of even larger proglacial lakes dammed by the coalescence of the BIIS and FIS during peak glacial phases has been hypothesised as well (e.g. Gibbard, 1995; Murton and Murton, 2012). The latter would have developed when northward-draining rivers were impounded by ice blocking northern outlets (Gibbard and Cohen, 2015), and drained during ice retreat, after which the southern North Sea became progressively inundated again during deglaciation as sea levels started to rise in response to melting ice sheets.

Until ca. 0.5 Myr ago, Britain was connected to mainland Europe even during these interglacial highstands via the Weald-Artois anticline, which diverted rivers draining southern England and northern France –such as the paleo-Solent, Somme and Seine– southwestward through the Channel River system between Cornwall and Brittany. More northerly rivers, including the Thames, Scheldt, Meuse and Rhine, discharged into the North Sea (Gibbard and Cohen, 2015). During MIS 12, impoundment of a large proglacial lake in the southern North Sea against the Weald-Artois ridge has been proposed to have led to overtopping, breaching, and erosion of this chalk barrier, progressively exposing weaker Eocene strata (e.g., London Clay). During MIS 6, a new proglacial lake has been proposed to have formed, impounded towards the southwest by a land bridge between East Anglia and Belgium, which may have been comprised of bedrock or remnants of a moraine (Gibbard, 2007) and located on top of the glacial forebulge. The subsequent drainage of this MIS 6 lake culminated in the final opening of the Dover Strait (Gibbard and Cohen, 2015). This two-stage breaching model builds on the concept of catastrophic drainage through the English Channel, first inferred from streamlined islands and longitudinal erosional grooves indicative of high-magnitude subaerial flooding, and Nd-isotopic evidence for meltwater injections into the Gulf of Biscay (Gupta et al., 2007; Collier et al., 2015; Toucanne et al., 2015), and later corroborated by the identification of overspill and plunge-pool features (Gupta et al., 2017). The final opening established a permanent North Sea-English Channel connection, diverting rivers such as the Thames and Scheldt southward; the Meuse and Rhine adopted this course after the last interglacial (Gibbard and Cohen, 2015).

The proposed location of a glacial forebulge between East Anglia and Belgium during MIS 6 (Gibbard and Cohen, 2015) has been invoked by De Clercq et al. (2018) to explain differences in relative sea-level history between Belgium and the Netherlands, as well as the tilting and westward deflection of the paleo-Scheldt

https://doi.org/10.5194/egusphere-2026-6213
Preprint. Discussion started: 26 November 2026
© Author(s) 2026. CC BY 4.0 License.

river valley north of Ghent, toward Zeebrugge and Ostend. However, they did not model the forebulge's precise location, elevation, or timing.

During the subsequent interglacial, i.e., the Eemian (MIS 5e), the southern North Sea coastline broadly resembled the present configuration, with Britain being separated from continental Europe for the first time (Gibbard and Cohen, 2015). Eemian sea level was ca. 4-9 m above the Holocene highstand (de Boer and van de Wal, 2021). Following MIS 5e, sea level fell overall, declining from ca. -25 m (MIS 5a), over ca. -90 m (MIS 4) to ca. -120 m (MIS 2) (Cohen et al., 2017).

Sedimentary evidence indicates two major periods of ice expansions during the last glaciation: one during MIS 4 and another during MIS 3/2 (Carr et al., 2006; Graham et al., 2011; Hughes et al., 2013). Although the Laurentide ice sheet peaked during the LGM, the Cordilleran, Barents-Kara and western Fennoscandian ice sheets reached their maximum extent already during MIS 4 (Ehlers et al., 2018) and the total Eurasian ice volume during MIS 4 was nearly comparable to that during the LGM. In Great-Britain, Ireland and the North Sea maximum ice extent occurred later, during MIS 2. The BIIS reached its maximum extent at 26 ka, when it started to merge with the FIS, while ice over the North Sea resulting from the confluence of British and Norwegian ice only reached its maximum extent at 22 ka (Clark et al., 2022b). The BIIS was substantially smaller than the FIS, which was one of the largest ice masses of the last glacial period. The FIS eventually merged with both the BIIS and the Barents-Kara ice sheet (Graham et al., 2011; Hughes et al., 2013; Svendsen et al., 2004) to form the third largest LGM ice complex after Antarctica and North America. This complex had a volume roughly three times that of the present-day Greenland Ice Sheet and contributed ca. 20 m to global sea-level lowering (Hughes et al., 2016; Patton et al., 2016).

Glaciolacustrine sediments, dated as MIS 3 to MIS 2, have been reported from the region of Dogger Bank by several authors (Cotterill et al., 2017; Roberts et al., 2018; Emery et al., 2019; Kyriakoudi et al., 2026), pointing to the presence –at least at some stage– of one or more proglacial lakes at the southern margin of the Weichselian ice sheet. Hjelstuen et al. (2018) identified evidence for drainage of an LGM ice-dammed lake that may have been located south of Dogger Bank, building on earlier suggestions of a northern drainage corridor during post-LGM retreat (Sejrup et al., 2016). The lake volume has been estimated at ~3900 km^3 (Bigg et al., 2012), with breaching occurring to the northeast of Dogger Bank at ca. 18.7 ka, when sea level was at least 110 m below present.

As ice loading induces subsidence beneath ice sheets, it seems plausible that GIA generated a topographic depression at the ice margin (e.g., Austermann et al., 2022), which may have helped determining the location of these Dogger Bank proglacial lakes, although this effect has not really been examined, modelled or discussed as a controlling factor so far, with most reconstructions prioritizing glaciogenic and topographic damming (Cotterill et al., 2017; Emery et al., 2019).

Ice loading not only causes subsidence beneath the ice sheets, but it also promotes the formation of a peripheral bulge. Kiden et al. (2002) placed the center of the Weichselian forebulge close to the Netherlands, although they only considered an ice load exerted by the FIS without contribution from the

https://doi.org/10.5194/egusphere-2026-6213
Preprint. Discussion started: 26 November 2026
© Author(s) 2026. CC BY 4.0 License.

BIIS. Similar conclusions were reached by Fjeldskaar (1994), who estimated 10-20 m of uplift in the region. However, estimates of forebulge magnitude and spatial evolution vary widely. Mörner (1979) proposed up to 170 m of postglacial subsidence, whereas Steffen and Wu (2011) modelled a forebulge of ~20 m high associated with the FIS, extending across northern Netherlands and Germany toward Dogger Bank. This geometry broadly accords with Kiden et al. (2002) and reconstructions by Busschers et al. (2007) for 21 ka based on data from the ICE-5G (VM2) model (Peltier, 2004) and from Steffen (2006). Vink et al. (2007) further demonstrated southwestward-decreasing and time-dependent subsidence related to FIS decay, consistent with spatial migration and progressive forebulge collapse. According to Le Meur (1996), forebulge amplitude approximates one-tenth of the central isostatic depression beneath the adjacent ice sheet.

The LGM lowstand was followed by a rapid termination and sea-level rise (de Boer and van de Wal, 2021). Post-LGM inundation progressed mainly north to south (Amkreutz et al., 2022), reflecting overall basin bathymetry.

3. MATERIAL AND METHODS

GIA modelling requires two principal inputs: an Earth rheological model and a prescribed surface load representing the spatiotemporal variations in ice and water masses over glacial cycles. In this study, which focuses on the last glacial cycle, hydro-isostatic loading was not included. This simplification is justified because much of the southern North Sea basin remained emergent from ~80 ka until the onset of the Holocene. Moreover, the water load in this region is small relative to the adjacent ice load. Present-day water depths across most of the North Sea do not exceed ~100 m, whereas former ice sheets reached thicknesses of several kilometres and had densities only slightly lower than seawater.

Excluding sea-level change also implies that rotational feedbacks are not considered. These feedbacks affect the geometry of the sea surface and the geoid (Milne and Mitrovica, 1998) and thereby contribute to solid earth deformation. Neglecting hydro-isostatic loading substantially reduces computational complexity by removing the need to solve the sea-level equation. Originally formulated by Farrell and Clark (1976), this equation describes the spatiotemporal evolution of relative sea level arising from meltwater redistribution and ice-ocean feedbacks, which impacts the solid Earth response to the combined ice and water loads. Solving the sea-level equation requires modelling interactions between global ice masses and spatially variable sea level, substantially increasing computational demands. The far-field signal resulting from ice masses such as those on North America or Antarctica was thus not accounted for. We argue that this signal would not vary significantly between different regions within our study area.

Instead, the GIA simulations presented here adopt the simplified Elastic Lithosphere-Relaxing Asthenosphere (ELRA) approach of Le Meur and Huybrechts (1996). In this framework, the lithosphere behaves elastically and accounts for flexural rigidity, while time-dependent mantle flow is parameterised through exponential relaxation representing a viscously relaxing asthenosphere. Compared with the self-

https://doi.org/10.5194/egusphere-2026-6213
Preprint. Discussion started: 26 November 2026
© Author(s) 2026. CC BY 4.0 License.

gravitating viscoelastic spherical Earth (SGVE) model of Le Meur (1996), the ELRA model is computationally far less demanding while producing comparable results.

3.1. GIA calculations

The Elastic Lithosphere-Relaxing Asthenosphere (ELRA) treatment of the solid Earth forms the basis of the GIA model applied here. The ELRA approach comprises two components. First, the equilibrium (steady-state) response to a prescribed load is calculated assuming an elastic lithosphere. Plate deflection is governed by flexural rigidity, which depends on lithospheric thickness. The equilibrium configuration is approached asymptotically following load emplacement, while the transient response is parameterised as exponential relaxation.

All calculations were performed in MATLAB® (The MathWorks Inc., 2022). Implementation of the steady-state Elastic Lithosphere component follows the scheme used in Kori-ULB (Coulon et al., 2021; Pattyn, 2017), an ice-flow model that incorporates GIA effects. The corresponding source code is publicly available.

3.1.1 Elastic Lithosphere component

Deflection of the elastic lithosphere, w, is governed by a fourth-order differential equation (Huybrechts and de Wolde, 1999; Le Meur and Huybrechts, 1996):

$$D\nabla^4 w + \rho_a g w = q \quad (1)$$

Here, D denotes the flexural rigidity (Pa m^3), calculated following Brotchie and Silvester (1969):

$$D = \frac{E T_e^3}{12(1-\nu^2)} \quad (2)$$

where E is Young's modulus (100 GPa), ν is Poisson's ratio (0.25), and T_e is the effective elastic lithosphere thickness (e.g., Tesauro et al., 2012). Le Meur and Huybrechts (1996) determined a flexural rigidity of 10^{25} Pa m^3 for their ELRA model calibrated against the SGVE model, corresponding to an effective lithospheric thickness of ~104 km.

Equation (1) further incorporates asthenospheric density ρ_a (3300 kg m^{-3}), gravitational acceleration g (9.81 m s^{-2}) and the applied ice load q. The latter depends solely on ice thickness h (m), gravitational acceleration, and ice density ρ_i (917 kg m^{-3}):

$$q = \rho_i g h \quad (3)$$

As demonstrated by Le Meur and Huybrechts (1996) and Huybrechts and de Wolde (1999), Eq. (1) can be solved for vertical lithospheric displacement w, as a function of the point load P_w ($= q\ x\ area$) and the distance r from the point load. Using the normalised distance $x = r/L_r$ the solution can be written as:

https://doi.org/10.5194/egusphere-2026-6213
Preprint. Discussion started: 26 November 2026
© Author(s) 2026. CC BY 4.0 License.

$$w(x) = \frac{P_w L_r^2}{2\pi D} kei(x) \quad (4)$$

Here, L_r denotes the radius of relative stiffness, or flexural length scale:

$$L_r = \left(\frac{D}{\rho_a g}\right)^{\frac{1}{4}} \quad (5)$$

This value depends on flexural rigidity –and thus lithospheric thickness– and is ~130 km for the chosen rigidity of 10^{25} Pa m^3. The function *kei(x)* is a zero-order Kelvin function, defined as the imaginary part of the modified Bessel function of the second kind (Brotchie and Silvester, 1969; Oldham et al., 2008). Equation (4) describes lithospheric deflection induced by a single point load; total deflection at a location is obtained by summing the contributions from all surrounding point loads.

3.1.2 Relaxing Asthenosphere component

The rate of change in vertical displacement is given by:

$$\frac{\delta w}{\delta t} = -\frac{1}{\tau_a}(w - w_{ss}) \quad (6)$$

where w_{ss} represents the steady-state or 'final' displacement toward which w decays exponentially if ice thickness remains constant. The relaxation time τ_a depends on asthenospheric properties and is set to 3000 years following the ELRA model of Le Meur and Huybrechts (1996), corresponding to an upper-mantle viscosity of 5×10^{20} Pa s.

The solution of Eq. (6) provides lithospheric displacement at time t after the onset of loading (e.g., Greve, 2001):

$$w(t) = w_{ss} + (w_0 - w_{ss})e^{\frac{-t}{\tau_a}} \quad (7)$$

where w_0 is the initial displacement at $t = 0$ and decays exponentially toward w_{ss} over time.

Ice thickness (h) from the ice sheet reconstructions is available only at temporal resolutions of 1 or 2.5 kyr. To increase temporal resolution, ice loads were linearly interpolated between neighbouring time slices at 100-year intervals. The lithosphere relaxes exponentially toward the applied load during each 100-year step before the next load is imposed. This iterative procedure continues until Termination I. A substantial difference in GIA response occurs between coarse time steps (1-2.5 kyr) and the 100-year interpolation, whereas further reducing the time step (e.g., to 10 years) produces negligible changes in GIA response.

3.2. Ice sheet reconstructions

The applied ice load (q) depends on ice thickness (h), which was derived from published reconstructions. We use the BRITICE-CHRONO reconstruction (Clark et al., 2022b) to calculate the GIA response throughout

https://doi.org/10.5194/egusphere-2026-6213
Preprint. Discussion started: 26 November 2026
© Author(s) 2026. CC BY 4.0 License.

the LGM. This reconstruction is constrained by geochronological data from the British Isles, the adjacent continental shelf and the North Sea. Ice extent, basal topography and basal shear stress were used as input for ICESHEET 1.0 (Gowan et al., 2016). As the BIIS interacted with the FIS, the domain was extended to include Norway, Denmark and Southern Sweden, following ice margins from the DATED-1 project (Hughes et al., 2016). The resulting output forced simulations with the Parallel Ice Sheet Model (Bueler and Brown, 2009; Winkelmann et al., 2011) to ensure consistency between ice dynamics and reconstructed thickness. Ice extent and thickness are available as GIS datasets at 1 kyr intervals from 31-15 ka (Clark et al., 2022a).

As European MIS 4 glaciation was also extensive, we use the PaleoMIST (Paleo ice sheet Margins, Ice Sheets and Topography) model (Gowan et al., 2021) to reconstruct the GIA signal during MIS 4 and MIS 3 and compare MIS 2 results with those derived from BRITICE-CHRONO. PaleoMIST is a global physics-based ice-sheet model constrained by geological evidence and relative sea-level data. Sea-level changes were computed using SELEN (Spada and Stocchi, 2007) and a 1D, spherically symmetric Earth model with a 120 km elastic lithosphere, upper mantle viscosity of 4×10^{20} Pa s and lower mantle viscosity of 4×10^{22} Pa s (Gowan et al., 2021). Ice sheets were reconstructed with ICESHEET (Gowan et al., 2016). Margins follow published reconstructions by Helmens (2014), Hughes et al. (2016) and Ingólfsson and Landvik (2013), with basal shear stress initialised from present-day geology and topography. The final PaleoMIST dataset spans 80 ka to present at 2.5 kyr resolution on a 5 × 5 km Lambert azimuthal equal-area grid (Gowan, 2019).

Several Eurasian ice sheet reconstructions extending to the onset of the last glacial period are available, including ICE-6G_C (Argus et al., 2014; Peltier et al., 2015) and RSES-ANU (Lambeck et al., 2006). Both derive from iterative solutions of the sea-level equation: ICE-6G_C updates the global model framework, whereas RSES-ANU refines individual ice-sheet components. The Näslund model (Näslund, 2010), based on the University of Maine Ice Sheet Model, is a regional thermo-mechanical reconstruction constrained by paleoclimate and topography. However, these models are older and have substantially lower spatial resolution than BRITICE-CHRONO and PaleoMIST. Prior to MIS 4, higher sea levels imply stronger hydro-isostatic contributions during the early part of the last glacial period, reducing the suitability of the ELRA approach. Accordingly, GIA simulations in this study are restricted to MIS 4-2 and employ the PaleoMIST and BRITICE-CHRONO reconstructions.

https://doi.org/10.5194/egusphere-2026-6213
Preprint. Discussion started: 26 November 2026
© Author(s) 2026. CC BY 4.0 License.

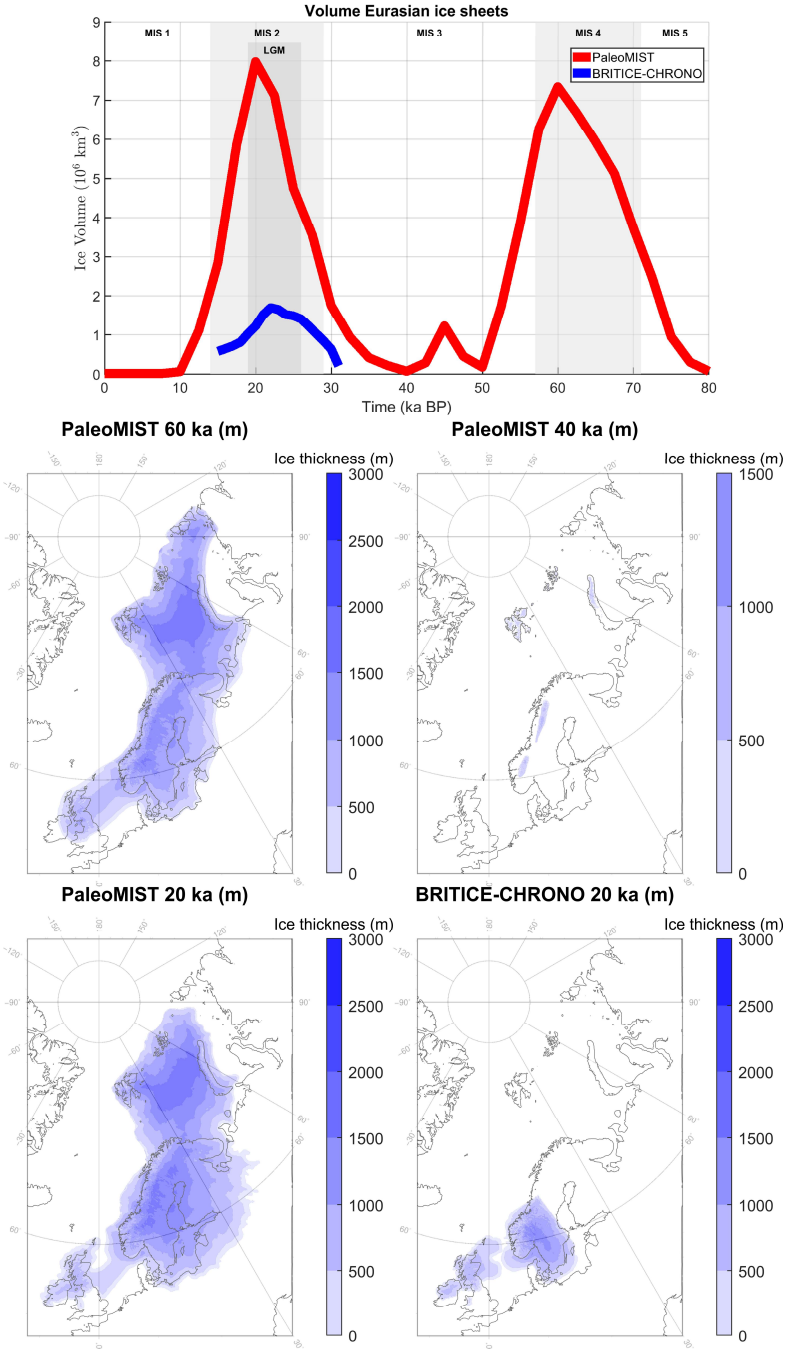

https://doi.org/10.5194/egusphere-2026-6213
Preprint. Discussion started: 26 November 2026
© Author(s) 2026. CC BY 4.0 License.

Figure 2: A) Evolution of ice volumes according to PaleoMIST (BIIS, FIS and Barents-Kara Ice Sheet, from 80 to 0 ka) and BRITICE-CHRONO (BIIS and southern FIS, from 31 to 15 ka). B) Ice cover at 60, 40 and 20 ka according to PaleoMIST and at 20 ka according to BRITICE-CHRONO.

Figure 2 illustrates ice sheet evolution in northwestern and northern Europe from 80 ka to present. PaleoMIST shows progressive ice growth between 80 and 60 ka, culminating in the MIS 4 maximum. Substantial retreat follows during MIS 3 before renewed expansion during MIS 2 leads to the LGM peak at ~20 ka. Ice volume during MIS 2 was only slightly greater than during MIS 4, and complete deglaciation occurred at the onset of the Holocene. For comparison, the BRITICE-CHRONO LGM reconstruction is also shown. Although total ice volume is lower –reflecting inclusion of only the BIIS and the southern sector of the FIS– the overall trend is similar. However, BRITICE-CHRONO indicates an earlier LGM peak at ~23 ka.

3.3. Sensitivity tests

To evaluate the effect of neglecting either the BIIS or FIS, vertical displacement was calculated for each ice sheet separately. Because BRITICE-CHRONO reconstructs only the BIIS and the southern part of the FIS, we additionally ran PaleoMIST over the same restricted domain to assess the implications for GIA modelling in the North Sea region.

A flexural rigidity of 10^{25} Pa m^3 was adopted, which corresponds to an effective lithospheric thickness of ~104 km. However, European lithospheric thickness remains debated. Estimates range from 71-95 km beneath the British Isles (Bradley et al., 2011; Milne et al., 2006) to strong lateral variability across western Europe, including ~140 km beneath Belgium, ~100 km beneath the Netherlands, and ~80 km along the northwest German coast (Vink et al., 2007). GPS-based studies suggest lithospheric thicknesses of ~120 km beneath Fennoscandia (Bergstrand et al., 2005; Lidberg et al., 2010). A sensitivity analysis therefore employed flexural rigidities of 3.0 x 10^{24} Pa m^3, 6.5 x 10^{24} Pa m^3 and 1.5 x 10^{25} Pa m^3, corresponding to lithospheric thicknesses of 70, 90 and 120 km, respectively.

An upper mantle viscosity of 5 × 10^{20} Pa s, corresponding to a time-constant of 3000 yr, is commonly used in GIA studies even when not employing the ELRA approach (e.g., Bradley et al., 2011; Lidberg et al., 2010; Milne et al., 2006). To assess model sensitivity, simulations were performed with relaxation times (τ_a) of 1000, 6000 and 10 000 yr, spanning the commonly accepted range of upper-mantle viscosities.

3.4. Data visualisation

The GIA signal was calculated for the entire North Sea region and mapped using a white-red colour scale with 1 m uplift contours and a white-blue scale with 20 m depression contours. Ice sheet extent (but not thickness) is overlain for reference.

To evaluate drainage, basin development, and associated depositional processes during the last glacial cycle, the GIA response was superimposed on modern bathymetry of the southern North Sea (51- 57 °N). Paleotopography was estimated by accounting for (i) eustatic sea-level change, (ii) sediment redistribution, and (iii) vertical isostatic adjustment. Owing to the complex and insufficiently resolved stratigraphy,

https://doi.org/10.5194/egusphere-2026-6213
Preprint. Discussion started: 26 November 2026
© Author(s) 2026. CC BY 4.0 License.

sedimentary units deposited and/or eroded from MIS 4 onward were not backstripped, but are considered qualitatively in the discussion. For example, it is important to note that Dogger Bank, as a geomorphological feature, was formed only during MIS 2, at ca. 23 ka (Cotterill et al., 2017; Emery et al., 2019), by glaciotectonic deformation of sediments deposited during MIS 3. The paleotopographic maps representing time slices prior to 23 ka thus incorrectly show the presence of Dogger Bank as a shallow-water area. Similarly, the shallow-water area located between the northern termination of the Axial Channel and the Outer Silver Pit is underlain by a considerable accumulation of post-LGM deposits. During time slices prior to that, this area was in reality likely deeper than suggested by the paleotopographic maps. In contrast, the Axial Channel itself already existed during MIS 4 (Vervoort et al., submitted), and its appearance on the maps is thus largely correct for all time slices presented here. Also Oyster Ground was likely a lower-lying area during the entire time interval covered by our reconstructions. Paleotopography (present-day bathymetry combined with the GIA signal) is displayed using a 10 m stepwise rainbow colour scale with GIA contours overlain. Areas below sea level at a given time step and hydrologically connected to the ocean are shown in grey to approximate paleocoastlines. Sea-level estimates follow Lambeck et al. (2014) for 15-35 kyr and Lambeck et al. (2002) for 35-80 ka. Although local deviations from the global signal likely occurred, regional sea-level reconstructions remain sparse and poorly constrained and would vary spatially across the southern North Sea basin.

4. RESULTS

4.1. Influence of ignoring ice masses

Displacement patterns derived from simulations including only the BIIS or FIS differ markedly from those incorporating both ice sheets. As shown in Fig. 3, the zone of maximum forebulge uplift is located over Scandinavia when forced solely by the BIIS, whereas the British Isles experience uplift when only the FIS is applied. In contrast, simulations including both ice sheets place the maximum uplift at 20 ka over the Netherlands and adjacent parts of Belgium and Germany. Although the FIS accounts for more than half of the uplift in this region across reconstructions, the BIIS contribution is substantial. Neglecting either ice sheet not only underestimates total uplift but also alters forebulge geometry and orientation, with important implications for paleo-drainage reconstructions.

https://doi.org/10.5194/egusphere-2026-6213
Preprint. Discussion started: 26 November 2026
© Author(s) 2026. CC BY 4.0 License.

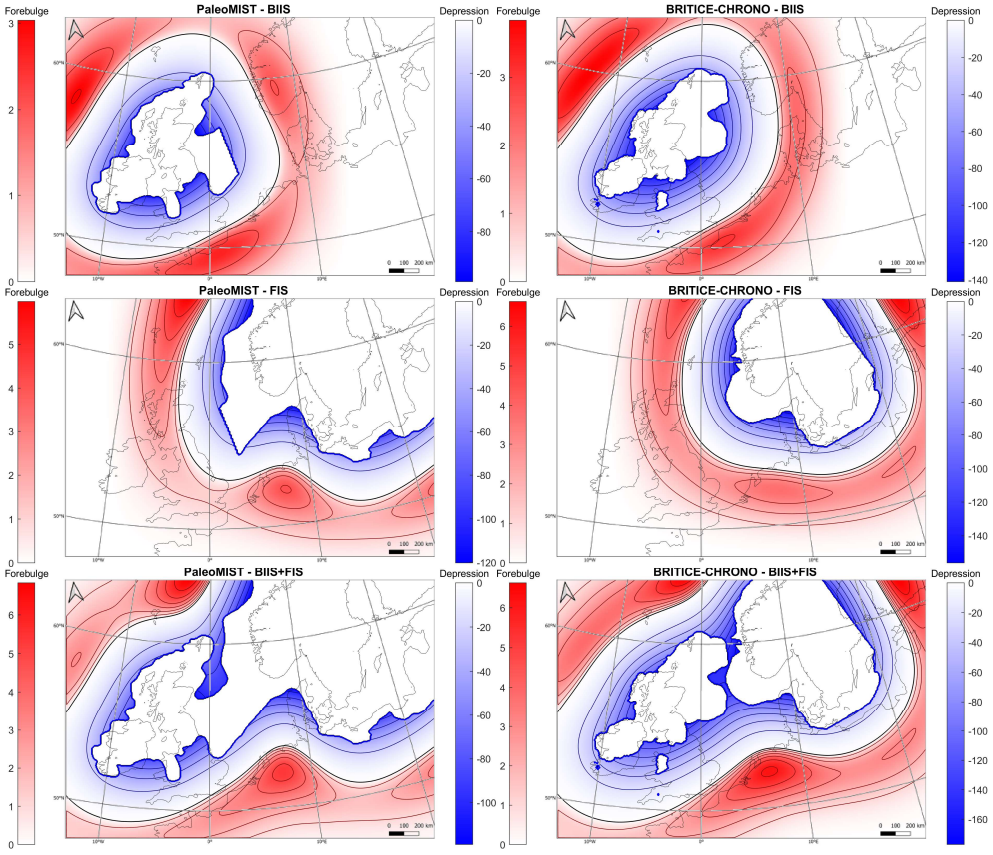

Figure 3: Vertical displacement (m) in the study area at 20 ka when considering only the BIIS, only the FIS and both the BIIS and FIS.

Figure 4 shows the GIA response at 20 ka obtained by forcing the model with the PaleoMIST reconstruction restricted to the same spatial domain as BRITICE-CHRONO. The negligible difference in vertical displacement relative to the full PaleoMIST simulation (Fig. 3) within the study area supports the validity of using the BRITICE-CHRONO reconstruction.

https://doi.org/10.5194/egusphere-2026-6213
Preprint. Discussion started: 26 November 2026
© Author(s) 2026. CC BY 4.0 License.

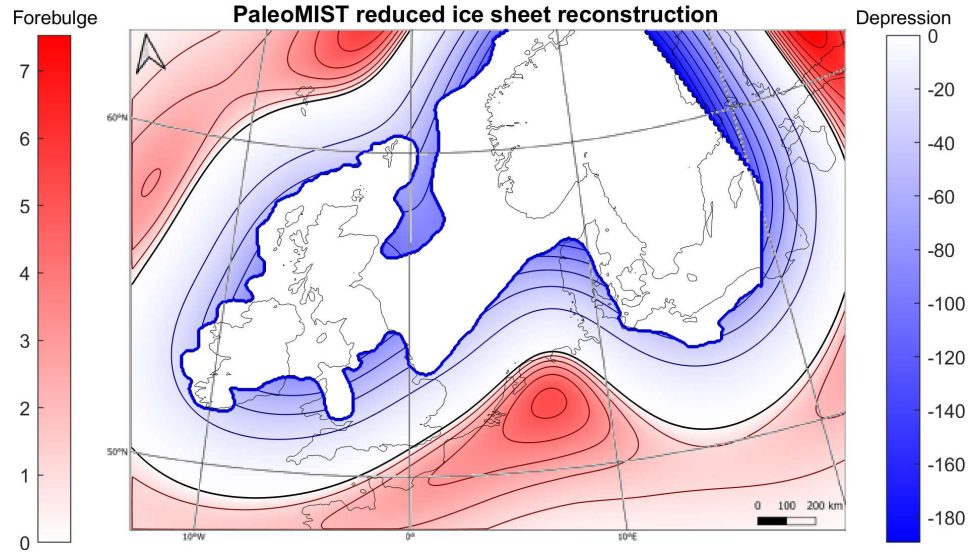

Figure 4: Vertical displacement (m) at 20 ka according to PaleoMIST based on the limited region used for the BRITICE-CHRONO reconstructions.

4.2. Sensitivity of Earth parameters

Simulations using both ice-sheet reconstructions with lithospheric thicknesses of 70, 90, and 120 km indicate that a thinner lithosphere produces greater depression beneath the ice sheet, whereas a thicker lithosphere generates a higher forebulge shifted farther away from the ice margin (Fig. 5).

https://doi.org/10.5194/egusphere-2026-6213
Preprint. Discussion started: 26 November 2026
© Author(s) 2026. CC BY 4.0 License.

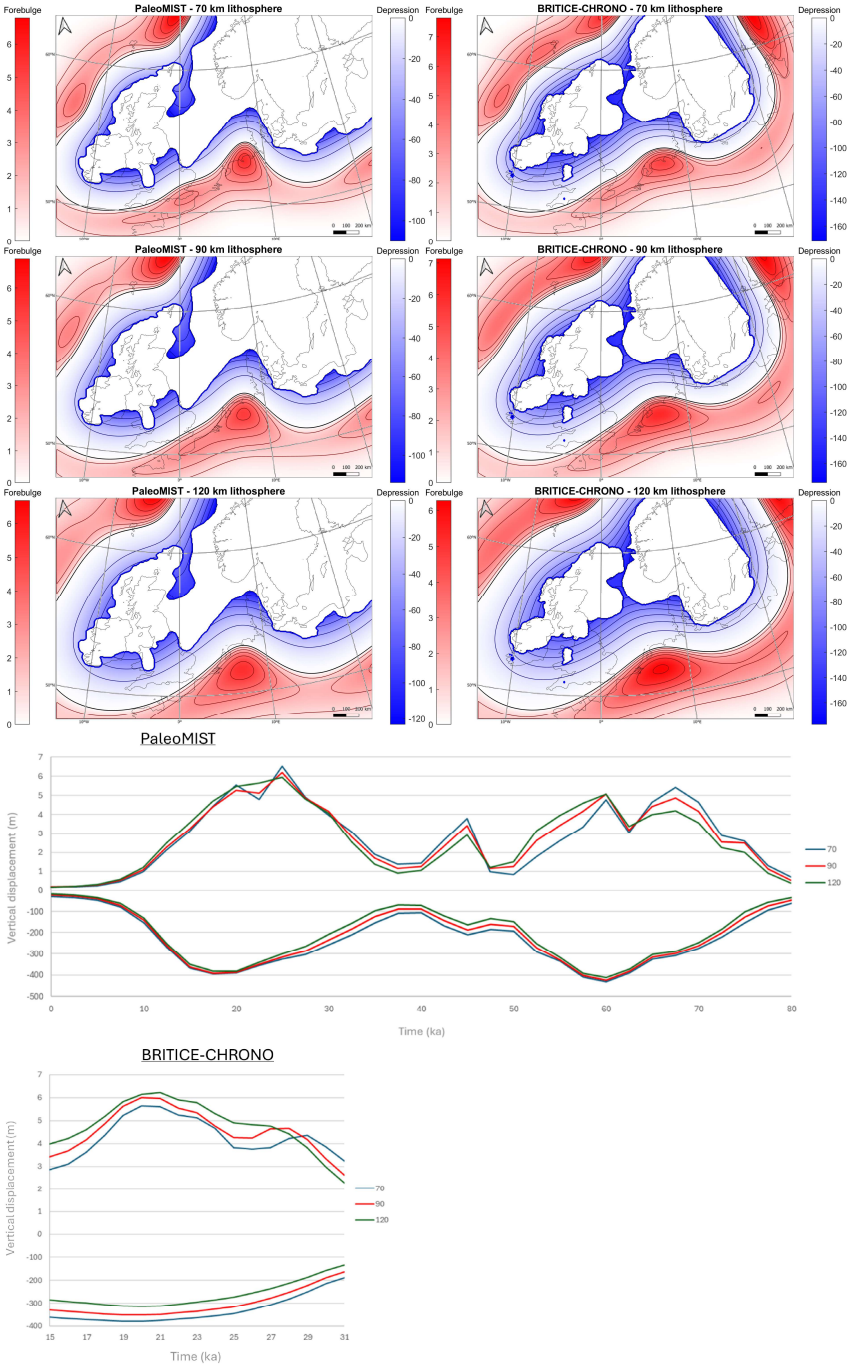

https://doi.org/10.5194/egusphere-2026-6213
Preprint. Discussion started: 26 November 2026
© Author(s) 2026. CC BY 4.0 License.

Figure 5: For lithospheric thickness values of 70, 90 and 120 km A) reconstruction of the vertical displacement (m) at 20 ka and B) evolution of maximal uplift in the region of interest and maximal depression over time.

Variations in asthenospheric viscosity are represented by changes in relaxation time. A shorter relaxation time produces larger vertical displacements during periods of extensive ice cover but smaller displacements during interstadials. In contrast, a longer relaxation time reduces vertical displacement and positions the forebulge closer to the ice sheet (Fig. 6).

https://doi.org/10.5194/egusphere-2026-6213
Preprint. Discussion started: 26 November 2026
© Author(s) 2026. CC BY 4.0 License.

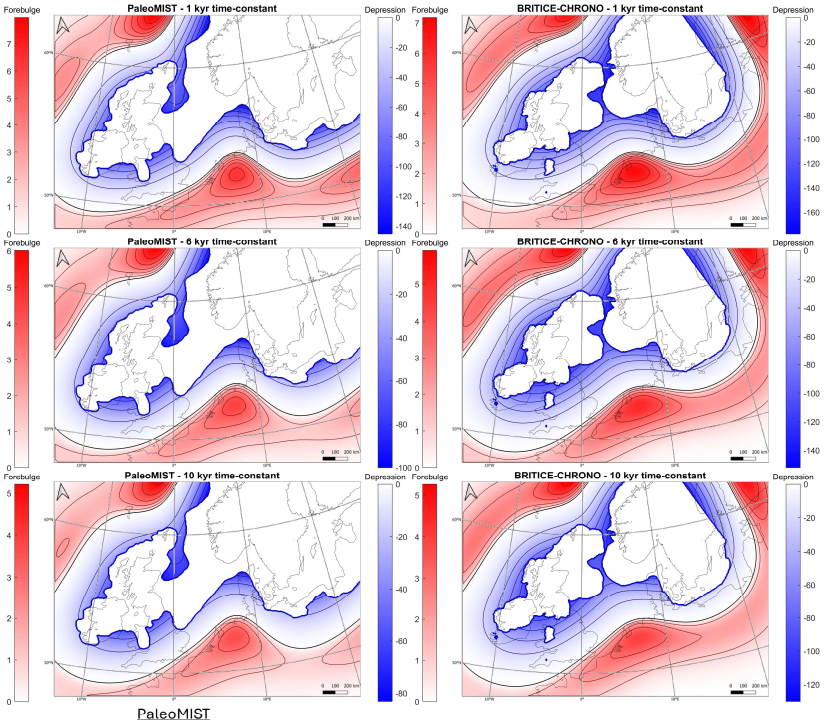

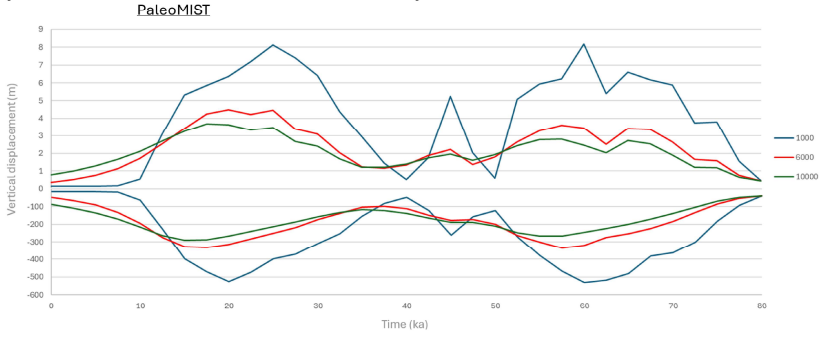

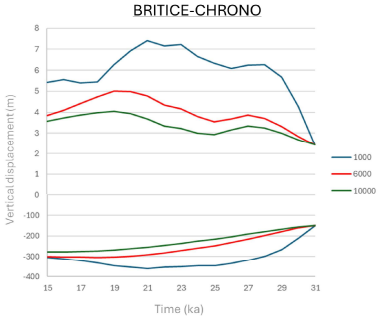

https://doi.org/10.5194/egusphere-2026-6213
Preprint. Discussion started: 26 November 2026
© Author(s) 2026. CC BY 4.0 License.

Figure 6: For time-constant values of 1000, 6000 and 10 000 years A) reconstruction of the vertical displacement (m) at 20 ka and B) evolution of maximal uplift in the region of interest and maximal depression over time.

4.3. GIA response in the North Sea region from MIS 4 to MIS 2

The GIA response was modelled from 80 to 15 ka using PaleoMIST and from 31 to 15 ka using BRITICE-CHRONO. According to PaleoMIST, ice first appeared on the British Isles shortly before the MIS 4 volume peak at 60 ka. Prior to this, a forebulge had developed around the FIS, extending through, a.o., southern Denmark and across the central North Sea toward the Orkney and Shetland Islands. This forebulge locally exceeded 4 m of uplift, whereas depression in the northern North Sea was on the order of several tens of meters (Fig. S1).

By 60 ka, the BIIS and FIS had merged over the North Sea, producing a forebulge apex exceeding 5 m in the central Netherlands (Fig. 7). Uplift in northern Belgium remained around 3-4 m. The hinge line between uplift and depression extended from the southeastern tip of England toward the Frisian Islands before turning southeast into Germany. Depression between this hinge line and the ice margin reached up to 60 m.

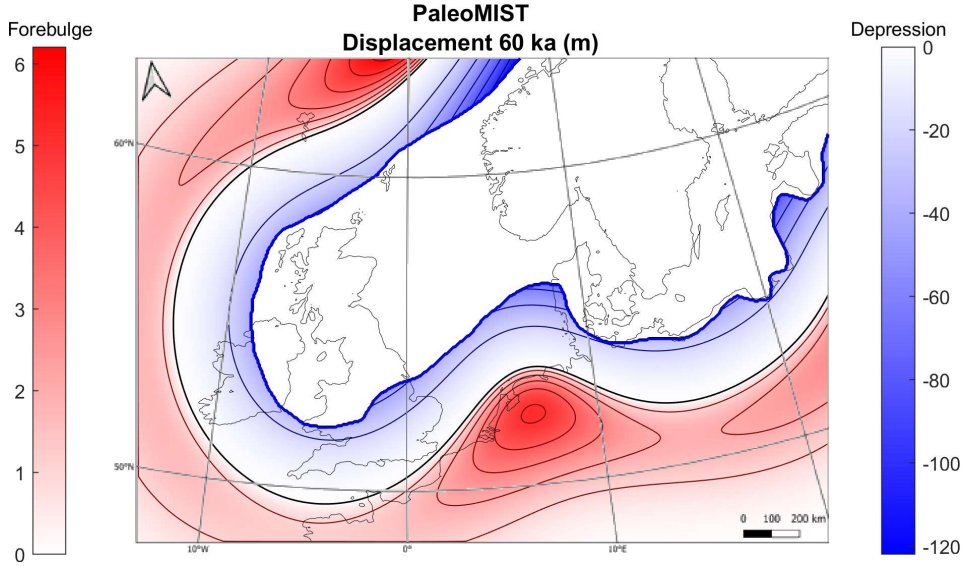

Figure 7: Reconstruction of the vertical displacement (m) at 60 ka based on the PaleoMIST ice sheet model.

A reduced or absent BIIS and a substantial retreat of the FIS until 30 ka caused the forebulge to migrate northwestward, even reconnecting with the forebulge north of Scotland across the North Sea, while overall vertical uplift and depression weakened (Fig. S1).

https://doi.org/10.5194/egusphere-2026-6213
Preprint. Discussion started: 26 November 2026
© Author(s) 2026. CC BY 4.0 License.

From 30 ka onward, BRITICE-CHRONO reconstructions become available. Both BRITICE-CHRONO and PaleoMIST indicate the presence of the BIIS, but the ice-free North Sea shifted the forebulge summit to the Dutch and German offshore sectors (Fig. 8).

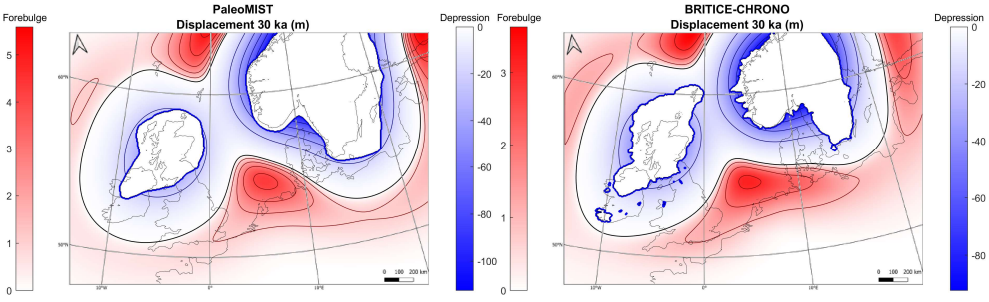

Figure 8: Reconstruction of the vertical displacement (m) at 30 ka based on the two ice sheet models.

The merging of the BIIS and FIS occurred at 29 ka in PaleoMIST and at 26 ka in BRITICE-CHRONO, driving the forebulge from the southeastern North Sea toward the Netherlands and northwestern Germany (Fig. S2). By 20 ka, BRITICE-CHRONO indicates a disconnection between the BIIS and FIS (Fig. 9). In both reconstructions, the forebulge hinge line passes through the southeastern tip of England, extends over the Frisian Islands, and turns southeast into Germany. The Netherlands experienced 5-6 m of uplift, whereas areas near the southern ice margin in the North Sea were depressed by up to ~100 m.

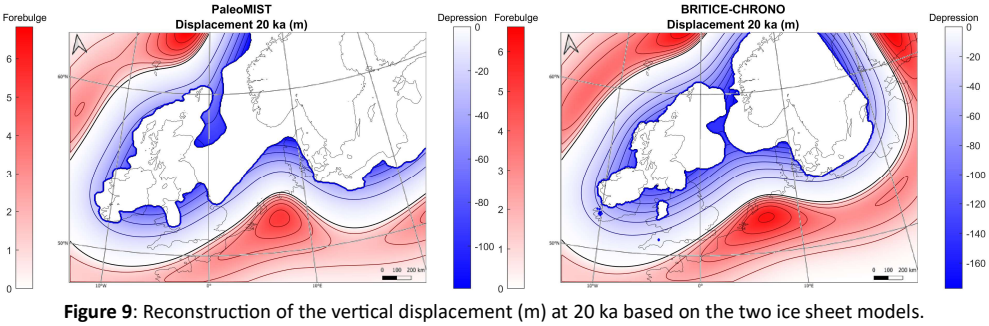

Figure 9: Reconstruction of the vertical displacement (m) at 20 ka based on the two ice sheet models.

Around 19 ka, PaleoMIST also indicates a disconnection between the BIIS and FIS (Fig. 10). The separation and rapid retreat of the ice sheets caused the hinge line to migrate toward the offshore sectors of the Netherlands and Germany. Once the ice had disappeared from the study area, lateral migration of the uplift-depression transition ceased. Thereafter, the lithosphere adjusted vertically toward the new ice-free equilibrium and is expected to relax exponentially toward zero displacement. At the same time, rising sea levels became increasingly important, initiating hydro-isostatic adjustment, which is not included in these models.

https://doi.org/10.5194/egusphere-2026-6213
Preprint. Discussion started: 26 November 2026
© Author(s) 2026. CC BY 4.0 License.

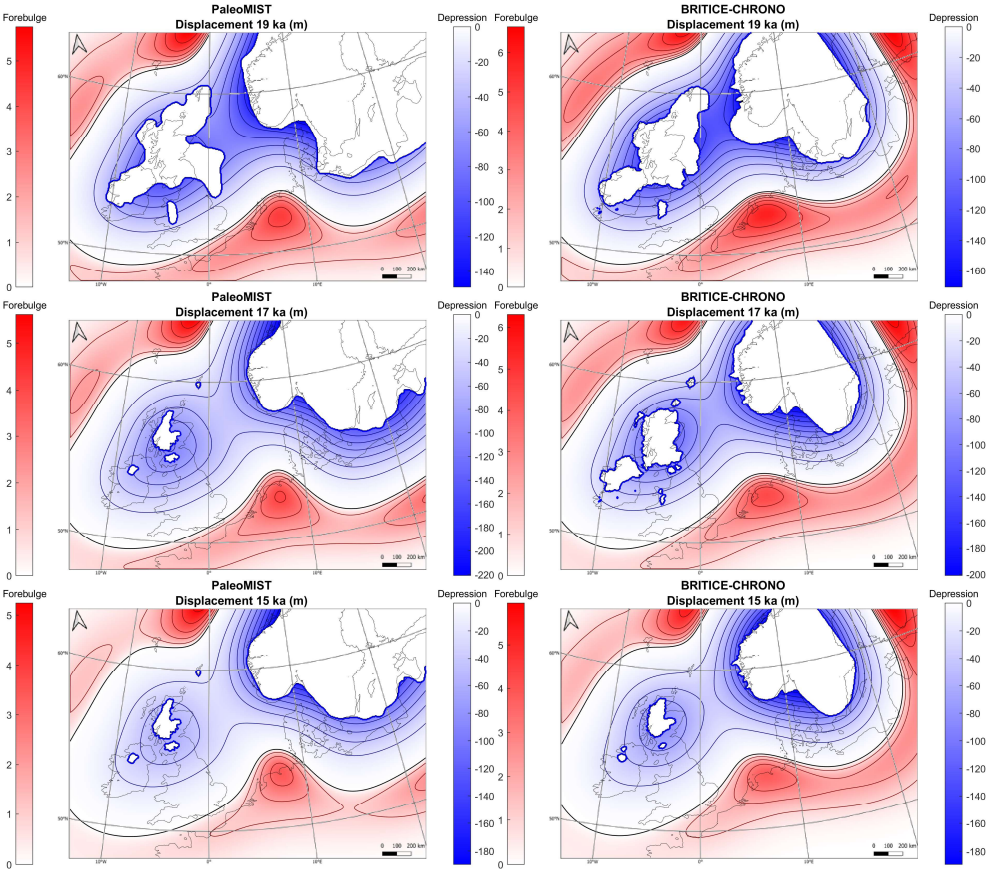

Figure 10: Reconstruction of the vertical displacement (m) at 19, 17 and 15 ka based on the two ice sheet models.

4.4. Paleotopographic reconstructions of the southern North Sea region from MIS 4 to MIS 2

From MIS 4 to MIS 2, parts of the region that presently form the North Sea were emergent. The modern bathymetry (Fig. 11) is compared with paleotopographic maps derived from the GIA reconstructions (Figs. 12-15), displayed using the same stepwise rainbow colour scale.

https://doi.org/10.5194/egusphere-2026-6213
Preprint. Discussion started: 26 November 2026
© Author(s) 2026. CC BY 4.0 License.

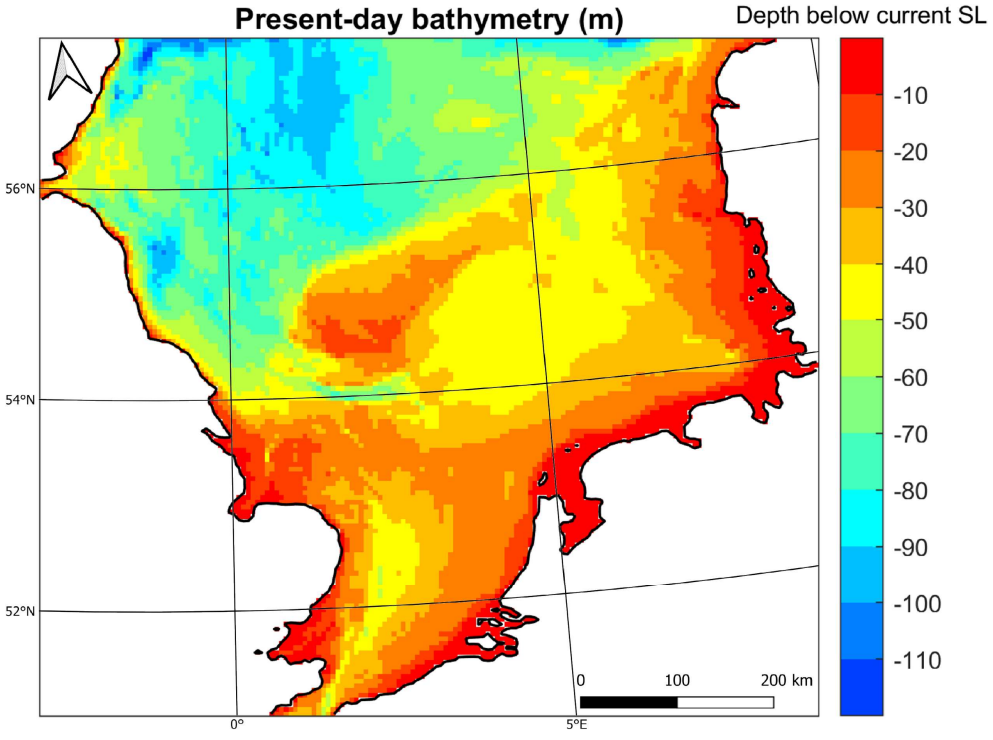

Figure 11: Current bathymetry map of the North Sea region covering the same area and using the same spatial resolution and colour scale as the paleotopography maps.

At 75 ka, relative sea level was ~60 m below the present interglacial level, placing the coastline just east of the modern British coast and northeast of Dogger Bank (Fig. 12). By 70 ka, well into MIS 4, glacial influence became significant in the study area. Although ice had not yet advanced into the region, the approaching ice sheets induced >20 m of depression in its northernmost parts. This, however, appears to not have significantly altered the orientation of the paleocoastline. A further sea-level fall of ~15 m by 65 ka led to the emergence of areas north of Dogger Bank.

https://doi.org/10.5194/egusphere-2026-6213
Preprint. Discussion started: 26 November 2026
© Author(s) 2026. CC BY 4.0 License.

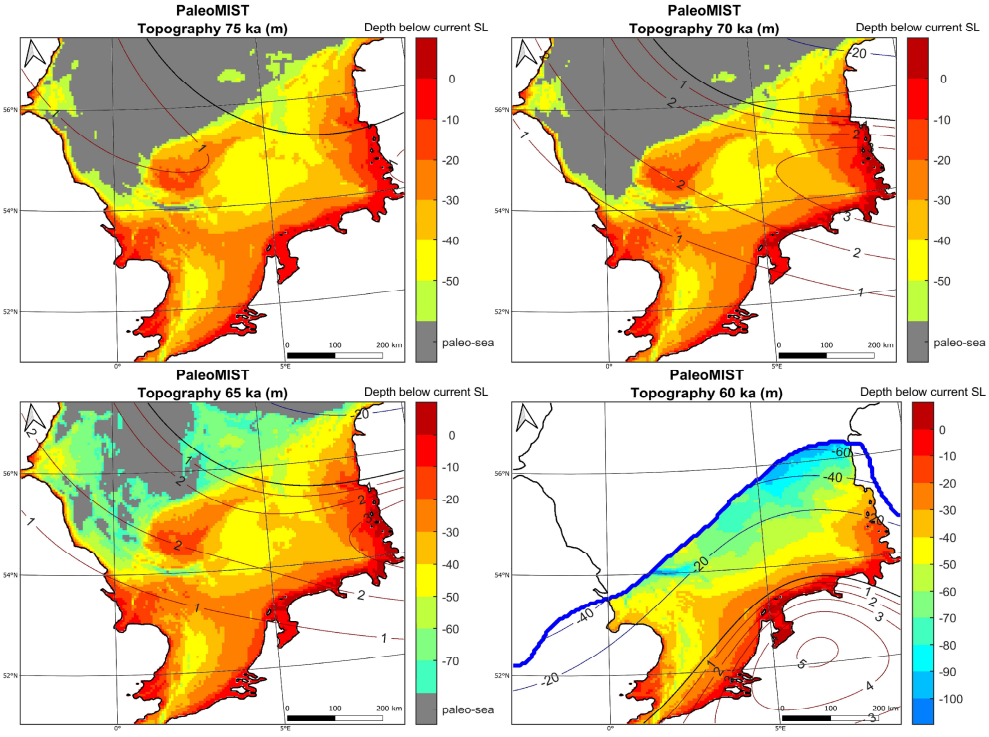

Figure 12: Evolution of the topography of the North Sea basin from 75 ka to 60 ka based on the current bathymetry and the GIA resulting from PaleoMIST, displayed using a 10 m stepwise rainbow colour scale. GIA contours are overlain at 1 m intervals for uplift and at 20 m intervals for depression. Areas below paleo-sea-level according to Lambeck et al. (2002) and hydrologically connected to the ocean are coloured grey. The ice margin is represented by a bold blue line. Note that Dogger Bank, as a geomorphological feature, only appeared during the LGM. The actual paleocoastlines during MIS 4-5 likely deviated slightly from what is shown here.

At 60 ka, the study area experienced full glacial conditions (Fig. 12). The British-Irish and Scandinavian ice sheets were coalescent, covering much of the North Sea. The southern ice margin trended SW-NE along the southern edge of Dogger Bank. As noted above, the Netherlands experienced ~5 m of GIA-related uplift, which also affected northern France, Belgium and parts of the present German coast. In the east, the ice margin crossed central Denmark. Immediately south of this margin, GIA-induced depression exceeded 60 m, placing the land surface up to ~100 m below present sea level.

By 55 ka, conditions had changed markedly. The BIIS had disappeared (and would not re-establish until ~30 ka) and the North Sea was ice-free (Fig. 13). The coastline again followed a SW-NE trend north of Dogger Bank. By 50 ka, the forebulge had largely decayed. Given that Dogger Bank did not exist around

https://doi.org/10.5194/egusphere-2026-6213
Preprint. Discussion started: 26 November 2026
© Author(s) 2026. CC BY 4.0 License.

this time, the North Sea might have reached further south than the northern edge of Dogger Bank. A subsequent sea-level fall at 40 ka led to renewed emergence of extensive areas north of Dogger Bank.

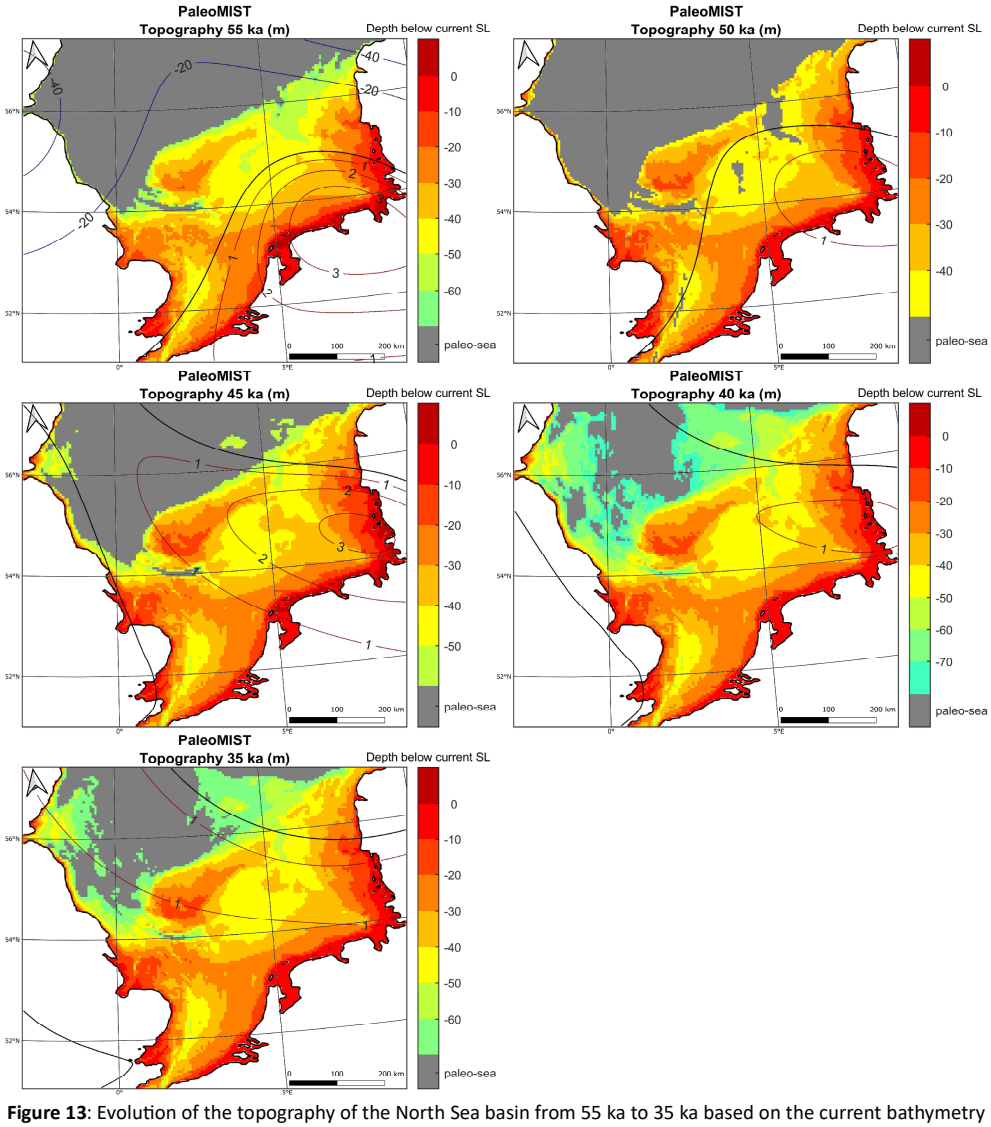

Figure 13: Evolution of the topography of the North Sea basin from 55 ka to 35 ka based on the current bathymetry and the GIA resulting from PaleoMIST, displayed using a 10 m stepwise rainbow colour scale. GIA contours are overlain at 1 m intervals for uplift and at 20 m intervals for depression. Areas below paleo-sea-level according to Lambeck et al. (2002) and hydrologically connected to the ocean are coloured grey. Note that Dogger Bank only appeared during the LGM. The actual paleocoastlines during MIS 3 likely deviated slightly from what is shown here.

https://doi.org/10.5194/egusphere-2026-6213
Preprint. Discussion started: 26 November 2026
© Author(s) 2026. CC BY 4.0 License.



At 30 ka, eustatic sea level fell to >100 m below present for the first time during the last glacial period and remained at least this low until ~15 ka. As a result, most of the study area was emergent (Fig. 14). At this time, the BIIS and FIS were still disconnected, and the forebulge apex over the Oyster Ground enhanced local elevation.

According to PaleoMIST, the BIIS and FIS merged at 29 ka, with a SW-NE-trending southern ice margin crossing Dogger Bank (Fig. 14). This margin migrated southward over the subsequent 7-8 kyr. When coalescence occurred at 26 ka in BRITICE-CHRONO, the forebulge in both reconstructions had shifted markedly southeastward, leading to depression of Dogger Bank and the Oyster Ground (Fig. 14). Maximum GIA-induced subsidence in the northernmost ice-free areas reached 40-60 m, placing parts of the southern North Sea at >100 m below present sea level.

https://doi.org/10.5194/egusphere-2026-6213
Preprint. Discussion started: 26 November 2026
© Author(s) 2026. CC BY 4.0 License.

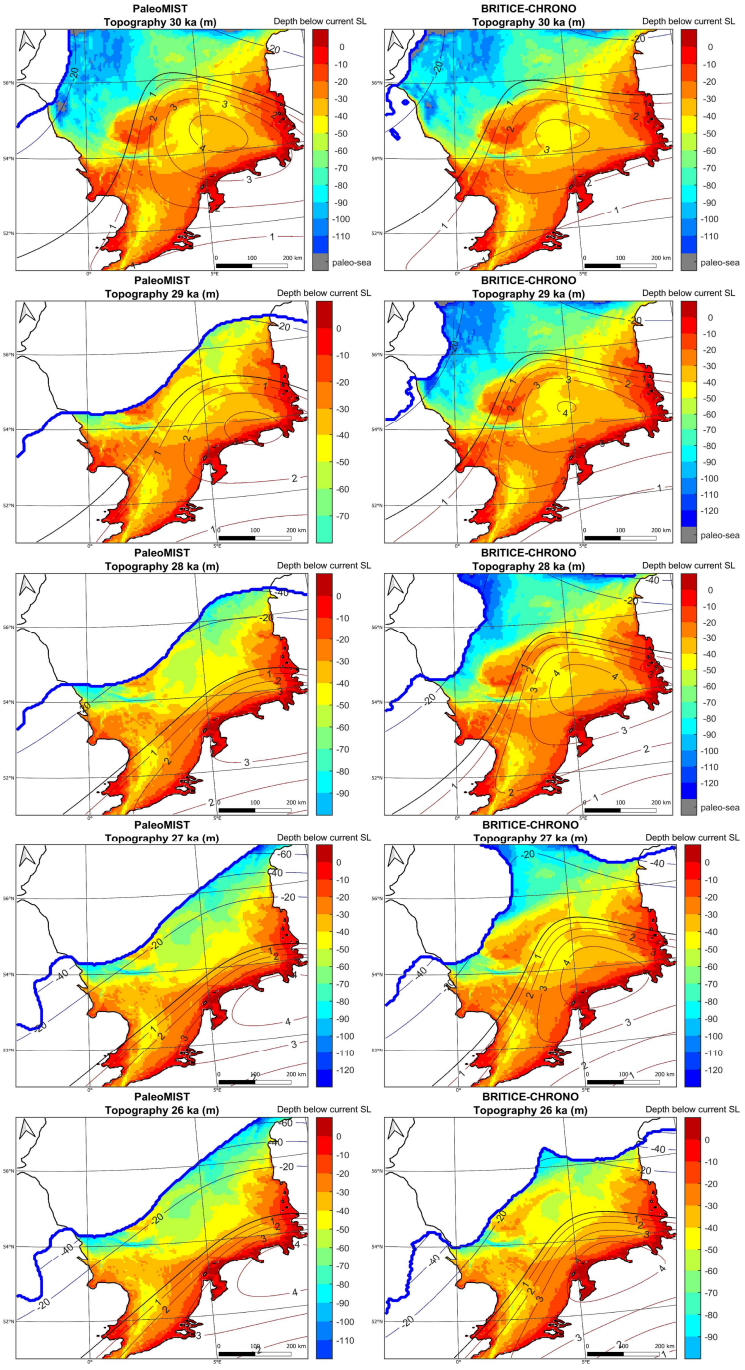

528

https://doi.org/10.5194/egusphere-2026-6213
Preprint. Discussion started: 26 November 2026
© Author(s) 2026. CC BY 4.0 License.

Figure 14: Evolution of the topography of the North Sea basin from 30 ka to 26 ka based on the current bathymetry and the GIA resulting from PaleoMIST and BRITICE-CHRONO, displayed using a 10 m stepwise rainbow colour scale. GIA contours are overlain at 1 m intervals for uplift and at 20 m intervals for depression. Areas below paleo-sea-level according to Lambeck et al. (2014) and hydrologically connected to the ocean are coloured grey. Ice margins are represented by bold blue lines. Note that Dogger Bank only appeared around 25-23 ka. The actual paleocoastlines during these time slices likely deviated slightly from what is shown here.

At the 23 ka BRITICE-CHRONO ice-volume maximum, both reconstructions indicate a southerly ice margin extending across Dogger Bank (Fig. 15), which likely formed during this timeframe (Emery et al., 2019). The topographic barrier between the Axial Channel and the North Sea, north of the Southern Bight, became further depressed in response to southward ice expansion. Immediately south of the ice margin, subsidence exceeded 100 m below present sea level.

Ice retreat began at 21 ka in BRITICE-CHRONO, exposing an ice-free basin reaching at least 170 m below present sea level. Retreat continued at 20 ka, when BRITICE-CHRONO first indicates separation of the BIIS and FIS, allowing marine inflow from the north into the deeply subsided area northwest of Dogger Bank and possible interaction with proglacial lake waters. PaleoMIST suggests a comparable marine connection slightly later, at 19 ka (Fig. 15).

As unloading reduced subsidence in the northern sector, isostatic rebound led to renewed emergence despite gradually rising eustatic sea level. This balance between sea-level rise and land uplift persisted until ~16-15 ka, when sea-level rise outpaced GIA-related uplift, resulting in progressive inundation of the southern North Sea.

https://doi.org/10.5194/egusphere-2026-6213
Preprint. Discussion started: 26 November 2026
© Author(s) 2026. CC BY 4.0 License.

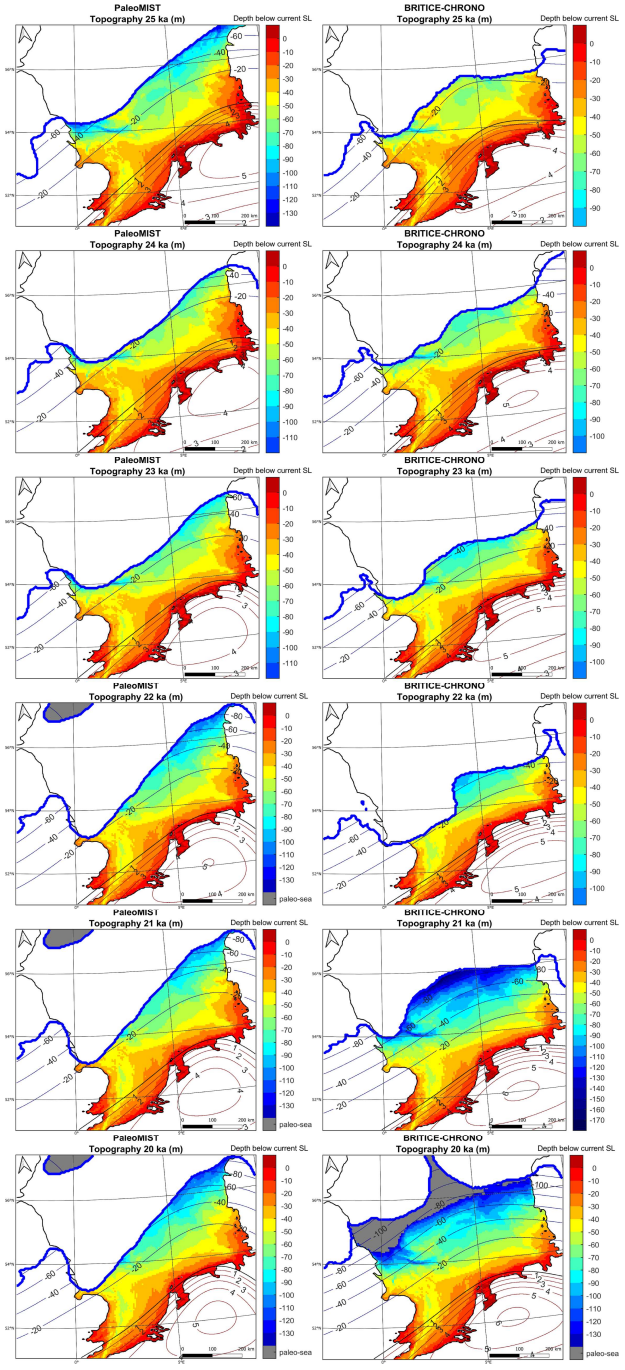

https://doi.org/10.5194/egusphere-2026-6213
Preprint. Discussion started: 26 November 2026
© Author(s) 2026. CC BY 4.0 License.

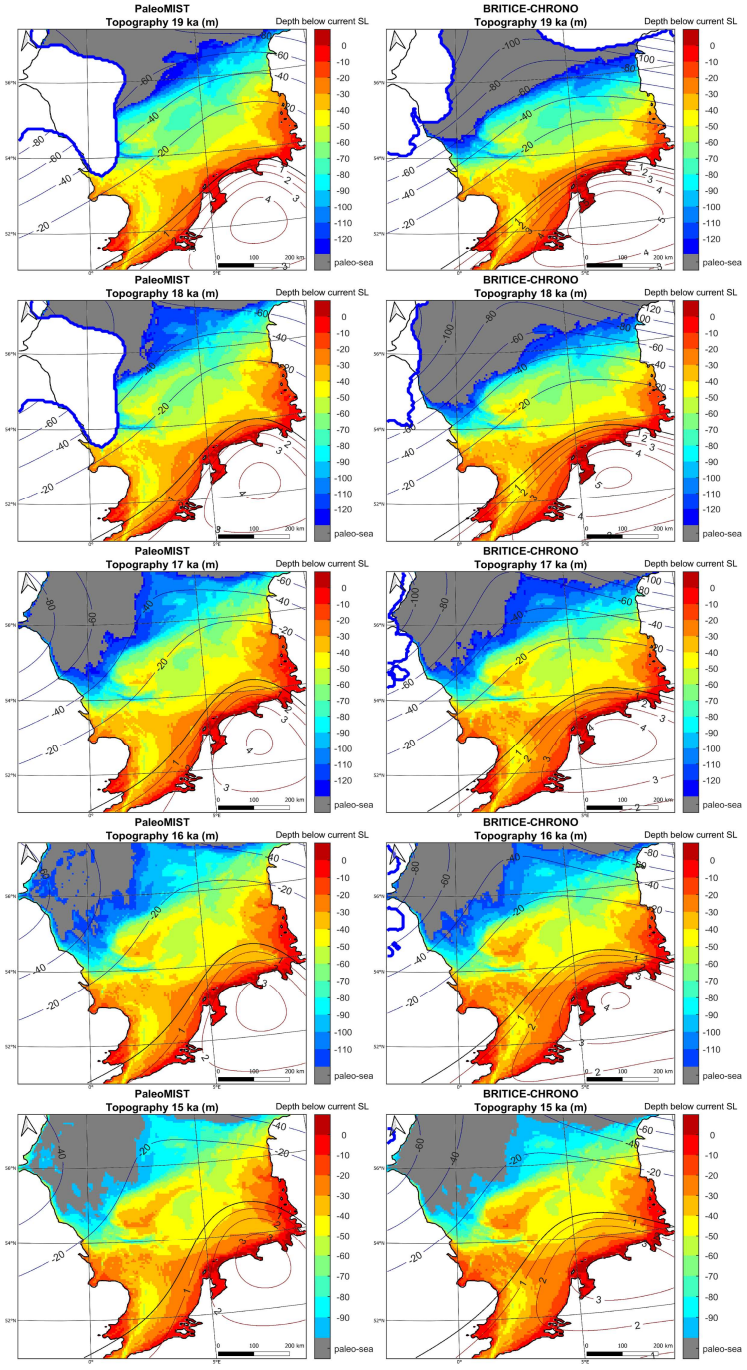

https://doi.org/10.5194/egusphere-2026-6213
Preprint. Discussion started: 26 November 2026
© Author(s) 2026. CC BY 4.0 License.

Figure 15: Evolution of the topography of the North Sea basin from 25 ka to 15 ka based on the current bathymetry and the GIA resulting from PaleoMIST and BRITICE-CHRONO, displayed using a 10 m stepwise rainbow colour scale. GIA contours are overlain at 1 m intervals for uplift and at 20 m intervals for depression. Areas below paleo-sea-level according to Lambeck et al. (2014) and hydrologically connected to the ocean are coloured grey. Ice margins are represented by bold blue lines. Note that Dogger Bank appeared around 25-23 ka.

5. DISCUSSION

5.1. Data sensitivity

Based on GIA calculations in which one of the ice masses is ignored, it can be concluded that neglecting either the BIIS or the FIS results in a serious misrepresentation of the total isostatic response to ice-sheet growth and retreat over time.

Lateral variations in forebulge location associated with changes in lithospheric thickness arise from differences in flexural rigidity. A thicker lithosphere, with higher rigidity, produces a longer bending wavelength in response to ice loading, whereas a thinner lithosphere results in stronger vertical displacement. This occurs because the ice-load signal is more strongly attenuated in a thicker lithosphere, which is more rigid and viscous than the asthenosphere.

Differences in the amplitude of vertical displacement across time constants directly reflect the relaxation time governing response damping. Short relaxation times produce a rapid response to ice loading, whereas longer relaxation times result in a response that is more distributed over time. Corresponding shifts in forebulge position can be attributed to ice-sheet build-up prior to 20 ka: short relaxation times primarily reflect ice configurations near 20 ka, whereas longer relaxation times are more strongly influenced by earlier, less extensive ice cover, placing the forebulge farther north.

Comparisons across lithospheric thicknesses and asthenosphere viscosities highlight contrasting sensitivities of the two layers. Forebulge migration varies little with relaxation time but responds strongly to lithospheric thickness, whereas the magnitude of vertical displacement is largely insensitive to lithospheric thickness and instead depends mainly on asthenosphere viscosity.

Vertical displacement patterns show that depression deepens toward the ice margin and is most pronounced beneath the ice sheets. Subglacial depression is not shown in the plots, as it lies outside the scope of this study and would obscure the ice extent. Depression attenuates toward the depression-uplift hinge line, whereas uplift is steepest on its ice-proximal side and decreases more gradually away from the ice sheet(s). Along ice margins, uplift is weakest at convex sections, strongest at concave sections, and intermediate along straight segments, reflecting divergence and convergence of displaced mantle material. This highlights the strong control of ice-sheet geometry on lateral displacement patterns and underscores the need for accurate ice-sheet reconstructions in GIA modelling.

5.2. Holocene and Lateglacial sediments

https://doi.org/10.5194/egusphere-2026-6213
Preprint. Discussion started: 26 November 2026
© Author(s) 2026. CC BY 4.0 License.

Because paleobathymetric data are limited, most GIA models rely on modern bathymetric maps to represent past topography. This can introduce discrepancies, as many depositional and erosional features formed relatively recently. Isopach maps derived from borehole data can partly account for this problem in coastal regions (Cohen et al., 2014), but such data are not always available. As noted earlier, recent sediments were also not backstripped in this study when constructing the paleotopographic maps.

Hoebe et al. (2024) developed a paleo-digital elevation model for the eastern part of the southern North Sea, covering the Belgian, Dutch and German onshore and offshore regions. This paleobathymetry represents the top of the Pleistocene and is based on multiple regional datasets. Differences between this model and modern bathymetry yield a Holocene sediment thickness map with a lateral resolution of 5 × 5 km and high vertical resolution. For the British sector of the North Sea, Holocene thickness data from the British Geological Survey are only partly available (Balson et al., 1991; Balson, 1988; Balson and D'Olier, 1990; Cameron et al., 1984; Harrison et al., 1987; Jeffery et al., 1988, 1990). Isopach maps mainly cover the central southern North Sea and extend only marginally into the western sector. Although their lateral resolution exceeds that of the Hoebe et al. (2024) grid, their usefulness is limited, due to sparse contouring, commonly restricted to 1, 5, 20 and 30 m intervals. Holocene sediment thickness north of Dogger Bank could therefore not be considered. Moreover, even accounting for Holocene sediments does not yield an exact MIS 4–MIS 2 paleotopography, as erosion and glaciogenic sedimentation during this period also modified the landscape.

Given these data limitations, only regional variations in Holocene thickness are considered here. North of the Axial Channel, Holocene sediments exceed 5 m in thickness and locally reach up to 15 m. Farther north, Holocene deposits at the eastern margin of Dogger Bank range from 5 to 20 m. Similar thicknesses occur in the German offshore sector, where sediments are concentrated along a NNW–SSE-trending depocenter, corresponding to the Elbe Paleovalley. During MIS 2, this valley routed meltwater from the Fennoscandian Ice Sheet and adjacent ice-free regions toward the Norwegian Channel (e.g., Özmaral et al., 2022), draining rivers such as the Eider, Elbe, Weser and Ems. This northward drainage could only occur in the absence of BIIS–FIS coalescence and without a proglacial lake in the North Sea (Özmaral et al., 2022). Valley incision likely accompanied activation under lowered sea levels, whereas postglacial inundation led to Holocene sediment infill (Hoebe et al., 2024). Additional Holocene deposits of 5 to >20 m occur in the Wadden Sea and major estuaries, including those of the Weser, Ems, Rhine, Meuse and Scheldt, whereas the sediment cover at the Frisian Front is negligible. Localised larger sediment thicknesses resulted from sandbank formation, such as offshore Belgium. Accounting for Holocene sediments north of the Axial Channel, at the eastern Dogger Bank margin, and along the Elbe Paleovalley is therefore essential for interpreting past drainage patterns based on (paleo)topographic constraints. These areas are indicated in Fig. S3.

Dogger Bank itself formed during the LGM (Cotterill et al., 2017; Emery et al., 2019) and it thus wrongly appears in paleotopographic reconstructions prior to its formation. As it was not possible to quantitatively backstrip Dogger Bank for the older time slices, its absence during our oldest reconstructions is considered qualitatively. The appearance of the Axial Channel as a channel feature is correct for all of our time slices, as it already existed during MIS 4 (Vervoort et al., submitted).

https://doi.org/10.5194/egusphere-2026-6213
Preprint. Discussion started: 26 November 2026
© Author(s) 2026. CC BY 4.0 License.

5.3. Drainage patterns during the last glacial period

During periods when the BIIS and FIS were merged, river drainage into the present-day North Sea basin was likely fundamentally different from periods when the ice sheets were separated and an ice-free corridor toward the northern North Sea existed.

The existence of one or more proglacial lakes at the southern margin of the merging ice sheets has been hypothesised by several authors (e.g., Sejrup et al., 2016), and possible evidence for northward drainage of such a lake after the LGM was presented by Hjelstuen et al. (2018). Hjelstuen et al. (2018) referred to Bigg et al. (2012) for lake volume estimates, which suggested a volume of approximately 3900 km^3. However, this estimate is based on maximum ice-sheet margins and present-day bathymetry and does not account for GIA. Moreover, the lake extent reconstructed by Bigg et al. (2012), spanning from the ice margin into the Southern Bight and covering much of the now-inundated area, is substantially larger than the lake reconstructed by Hjelstuen et al. (2018).

Based on isotopic data from a core at the northern North Sea margin and comparison with other regional records, Lekens et al. (2006) found evidence of meltwater release in the southern Norwegian Sea around 34 ka that was not related to Heinrich events. This timing coincides with the proposed northward drainage of the proglacial North Sea lake suggested by Bigg et al. (2012), but not with the post-LGM drainage proposed by Hjelstuen et al. (2018), which was attributed to ice-sheet unzipping. Both the PaleoMIST and BRITICE-CHRONO reconstructions indicate ice-sheet merging only after 30 ka and therefore do not support proglacial lake drainage around 34 ka.

Research on the now-inundated Elbe Paleovalley –also known as the Elbe Urstromtal or Heligoland Channel– is limited. The area was first mapped by Figge (1980), and it is generally assumed that valley formation and enlargement occurred primarily during MIS 2. This is attributed to outwash and meltwater delivery from the nearby FIS, as well as drainage from eastern, western and central Europe (Özmaral et al., 2022; Papenmeier and Hass, 2020; Westaway and Bridgland, 2010). Although there is no direct evidence for its existence during earlier glaciations, it is likely that during the Saalian and subsequent sea-level lowstands, the Elbe and Weser drained in broadly similar directions.

At the end of the Last Interglacial, when sea level was slightly higher than today, the Elbe and Weser likely entered the North Sea near their present-day mouths. In contrast, more southerly rivers followed different courses. The Rhine entered the North Sea farther north, east of the present-day Lake IJssel, as areas to the west were inundated, whereas the Meuse estuary was located southwest of the Rhine but still north of its modern mouth (Busschers et al., 2007). The Scheldt reoccupied its paleovalley, flowing westward north of Ghent toward Zeebrugge and Ostend (De Clercq et al., 2018). This incised valley formed at the end of the penultimate glaciation, likely due to GIA-related forebulge uplift followed by subsidence, and evolved into an estuary and seaway during the Eemian. Subsidence of the Saalian forebulge caused Eemian transgression to lag behind eustatic sea-level rise (De Clercq et al., 2018), a pattern commonly observed in the southern North Sea, although such transgressions proceeded rapidly (Cohen et al., 2017).

https://doi.org/10.5194/egusphere-2026-6213
Preprint. Discussion started: 26 November 2026
© Author(s) 2026. CC BY 4.0 License.

At the MIS 5–MIS 4 transition (~75 ka), the study area experienced its first glacial influence. This likely caused an increase in river discharge due to meltwater input, while river courses remained largely unaffected because GIA effects were still limited.

According to PaleoMIST, coalescence of the BIIS and FIS over the North Sea occurred around 60 ka. This event would have blocked northward drainage of rivers such as the Elbe and Weser, while meltwater input from the FIS increased. Ice blockage may therefore have led to the formation of a proglacial lake, with the ice margin forming its northern boundary (Fig. 16). GIA likely further deepened the basin, with the forebulge located southeast of the lake. The confluence of the Elbe and Weser, together with other FIS meltwater pathways, formed the main tributaries. Once filled, lake overtopping would have resulted in southward drainage via the topographically depressed Axial Channel. Combined with discharge from the Rhine, Meuse, and Scheldt, this water was then routed through the Dover Strait to the Atlantic Ocean. The Rhine and Meuse were characterized, at that time, by lateral migration and reworking, including reoccupation and widening of older braided channels (Busschers et al., 2007). The Rhine, in particular, widened substantially in the IJssel basin before being deflected southward, where it likely joined the Meuse prior to entering the Axial Channel. However, this inferred pathway appears inconsistent with paleotopography, which suggests a more northwesterly flow direction. Consequently, definitive conclusions regarding the Rhine's course during MIS 4 cannot be drawn.

The existence of a proglacial lake during MIS 4 was also proposed by De Clercq (2018), who suggested that lake overtopping may have triggered a glacial lake outburst flood (GLOF) or a cascade of GLOFs into the Axial Channel. Further evidence is required to substantiate this hypothesis, as the magnitude of southward drainage would have depended on meltwater supply rates, the stability of the overtopping threshold, and the paleotopography of the Axial Channel during MIS 4. The maximum volume of the proposed lake, calculated from the paleotopography shown in Fig. 16 but without backstripping of the Holocene and uppermost Pleistocene sediments, is estimated at ~1130 km^3, approximately 3.5 times smaller than the MIS 2 lake volume calculated by Bigg et al. (2012).

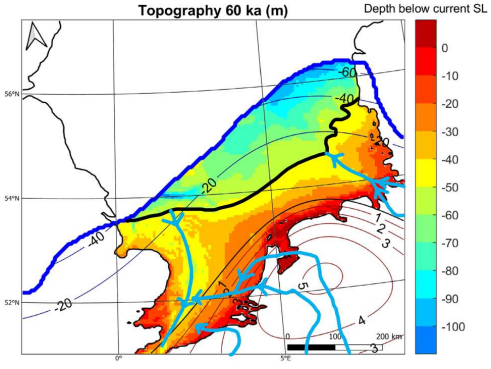

https://doi.org/10.5194/egusphere-2026-6213
Preprint. Discussion started: 26 November 2026
© Author(s) 2026. CC BY 4.0 License.

Figure 16: Assumed hydrological situation of the southern North Sea basin at 60 ka. Southern proglacial lake limit (bold black line) based on paleotopography (combination of current bathymetry and the GIA resulting from PaleoMIST, displayed using a 10 m stepwise rainbow colour scale) and on the known existence of Holocene sediments. GIA contours are overlain at 1 m intervals for uplift and at 20 m intervals for depression. Ice margin represented by a bold dark blue line, main river pathways depicted in light blue. Courses of Scheldt river and Meuse and Rhine rivers based on De Clercq et al. (2018) and Busschers et al. (2007) respectively, courses of Weser and Elbe rivers as well as southward drainage of the assumed proglacial lake based on paleotopography.

After the MIS 4 peak, ice-sheet retreat may have temporarily enlarged the lake basin, although this effect was counteracted by the subsequent attenuation of the GIA-related depression. The lake likely drained only partially to the south (i.e., by overtopping), as complete southward drainage would have required a reversal of regional topography. Once the BIIS and FIS unzipped, the remaining lake water would have drained northward into the North Sea.

Sedimentological evidence suggests a short-lived marine incursion into the Axial Channel around 50 ka (Vervoort et al., submitted). Our reconstructions also place the Axial Channel partially below sea level around this time, however with no marine connection in the north. When taking into account the presence of Holocene and Lateglacial sediments north of the Axial Channel that were not backstripped here (see also Fig. S3), as well as potential local deviations from the global sea level reconstructions used here, it is plausible that a marine incursion into the Axial Channel occurred around 50 ka.

At the onset of MIS 3, the Rhine partly avulsed and merged with the Meuse in the central Netherlands (Busschers et al., 2007). This new course was shorter and had a higher gradient, attributed to aggrading channel belts and increased sediment supply (Busschers et al., 2007). By this time, the forebulge had already migrated northward in response to ice-sheet retreat, placing the Rhine entirely on its southern flank. Although forebulge uplift was limited to a few meters, the resulting gradient may have further favoured a more southerly course, as also suggested by Busschers et al. (2007). The Scheldt, Meuse, Weser and Elbe likely followed courses similar to those during MIS 4, except that the Weser and Elbe drained directly into the North Sea rather than into a proglacial lake. The northern Rhine course was abandoned around 35 ka (Busschers et al., 2007).

At the MIS 3–MIS 2 transition (~30 ka), the North Sea region was likely still mostly ice-free, although renewed expansion of both the BIIS and FIS redirected increasing volumes of meltwater toward the study area. During this period, the Elbe Paleovalley likely began to develop. The Weser and Elbe, together with FIS meltwater, drained toward the still-inundated Norwegian Channel via this newly formed valley, which was occupied by a braided river system (Özmaral et al., 2022). In contrast, the Scheldt, Meuse and Rhine continued to drain southward via the Axial Channel, with the Rhine confined to its southernmost pathway.

At the onset of MIS 2, the BIIS and FIS merged again, preventing northward drainage of FIS meltwater and northwestern German rivers toward the Norwegian Channel. A westward deflection of this drainage toward the southern North Sea and subsequently southward via the Axial Channel has been proposed by Ménot et al. (2006) and Toucanne et al. (2010). Toucanne et al. (2010) suggested that this southwestward

https://doi.org/10.5194/egusphere-2026-6213
Preprint. Discussion started: 26 November 2026
© Author(s) 2026. CC BY 4.0 License.

drainage persisted from 30 to 18 ka, whereas Ménot et al. (2006) proposed a change only at ~17 ka. Both studies linked this drainage reorganisation to the presence of one or more proglacial lakes south of the ice margin. Based on paleogeographic reconstructions showing inundation of the Norwegian Channel since ~24 ka (Houmark-Nielsen and Kjær, 2003), Hijma et al. (2012) suggested northward rerouting of the Elbe from that time onward. However, this interpretation is not supported by the paleotopographic reconstructions presented here, which indicate that northward rerouting did not occur before ~20 ka.

Using neodymium isotopes, Toucanne et al. (2015) found evidence for major meltwater injections into the English Channel from the onset of BIIS–FIS coalescence until their unzipping, as well as sediment delivery to the Bay of Biscay. These events were attributed to episodic phases of intense ice melting during ice-sheet merging. In addition, García-Moreno (2017) identified erosional features in the Dover Strait formed during the final phase of valley incision at the LGM, most likely between 30 and 18 ka, providing evidence for a megaflood. Together with earlier hypotheses (Ménot et al., 2006; Toucanne et al., 2010) and the paleotopographic reconstructions presented here, this evidence strongly suggests that southwestward drainage from the southeastern North Sea basin was accompanied by the formation of one or more proglacial lakes that drained via the Axial Channel toward the Dover Strait and the Atlantic Ocean through the Channel River. The timing of individual GLOF events inferred by Toucanne et al. (2015) likely depended on breaching or overtopping of the lake, controlled by the interplay between meltwater supply and the GIA-dependent lake storage capacity.

Maximum proglacial lake storage capacity was quantified using the same approach as for the 60 ka time slice, but employing BRITICE-CHRONO-based paleotopographic reconstructions for the LGM, which are more recent and better constrained. Maximum lake extents and drainage pathways are reconstructed for 26, 23 and 21 ka (Fig. 17). Even though small-scale proglacial lakes could have formed in front of the ice margin prior to merging of the BIIS and FIS, only a larger lake basin with higher water levels could have caused the southwestward large magnitude floods, as evidenced by the erosional features observed in the Dover Strait. The 26 ka time slice represents the earliest phase of ice-sheet merging according to BRITICE-CHRONO and thus the first opportunity for the formation of a larger proglacial lake; 23 ka represents an intermediate stage, while after 21 ka ice-sheet unzipping precluded further lake existence. Shortly before unzipping and subsequent northward drainage, this proglacial lake must have been large (3900 km^3 according to Bigg et al., 2012 and Hjelstuen et al., 2018).

At 26 ka, the maximum lake volume is estimated at ~965 km^3, with a lake level approximately 40 m below present-day sea level. Higher lake levels would have resulted in overtopping and drainage toward the Axial Channel. Dogger Bank appears as an island at this stage (Fig. 17A), although the presence of substantial Holocene sediment cover must be considered, as well as the fact that Dogger Bank probably only formed a few thousand years later (Cotterill et al., 2017; Emery et al., 2019). Whether the basin was fully filled depends on meltwater supply, with initial filling occurring in the north, where former Elbe and Weser drainage entered the deepest part of the basin. Outflow to the south would only have been possible once the basin was fully filled, although semi-separated sub-basins may have existed during intermediate stages.

https://doi.org/10.5194/egusphere-2026-6213
Preprint. Discussion started: 26 November 2026
© Author(s) 2026. CC BY 4.0 License.

By 23 ka, southward migration of the ice margin covered Dogger Bank, and increased GIA-related depression lowered the overtopping threshold to ~50 m below present-day sea level (Fig. 17B). The maximum lake volume at this time is estimated at ~765 km^3. Despite greater overall depression, lake volume decreased due to the southward advance of the ice margin.

By 21 ka, shortly before BIIS–FIS unzipping, substantial northward retreat of the ice margin greatly enlarged the basin, particularly in the strongly depressed northern sector. At this stage, the basin could be filled to ~60 m below present-day sea level, yielding an estimated lake volume of ~3040 km^3. This value is comparable to the ~3900 km^3 estimated by Bigg et al. (2012) although the present estimate is based on depressed paleotopography rather than modern bathymetry. The volume is also comparable to that of Glacial Lake Missoula (~2184 km^3), which drained into the Pacific Ocean by multiple GLOFs between 15 ka and 13 ka (Clarke et al., 1984; O'Connor and Baker, 1992). A significant increase in lake volume during deglaciation—compared to glaciation—has been attributed to the lag in GIA response and the separation between the ice margin and the peripheral bulge for proglacial lakes bordering the Laurentide Ice Sheet as well (Austermann et al., 2022).

It is likely that the basin at 21 ka became fully filled. Rapid ice retreat would have supplied large volumes of meltwater directly from the southern North Sea ice margin and via proglacial rivers. The presence of the lake may itself have enhanced ice retreat by promoting flotation and calving (e.g., Austermann et al., 2022), whereas in its absence, the ice sheet would have been grounded on the exposed North Sea basin. At the onset of ice-sheet unzipping, excess meltwater likely drained southward, leaving behind a glacial outwash plain. Once the ice sheets separated, a deeply depressed northern outlet provided a favourable pathway for rapid draining of the remaining lake water as a GLOF. The exact timing of this event remains uncertain. While BRITICE-CHRONO indicates an ice-free northern corridor at ~20 ka, Hjelstuen et al. (2018) proposed drainage at ~18.7 ka based on ice-extent reconstructions by Sejrup et al. (2016). Subsequent lake drainage and ice retreat allowed reoccupation of the Elbe Paleovalley and reconnection with the Norwegian Channel, until final inundation during the Early Holocene (e.g., Hoebe et al., 2024; Özmaral et al., 2022).

https://doi.org/10.5194/egusphere-2026-6213
Preprint. Discussion started: 26 November 2026
© Author(s) 2026. CC BY 4.0 License.

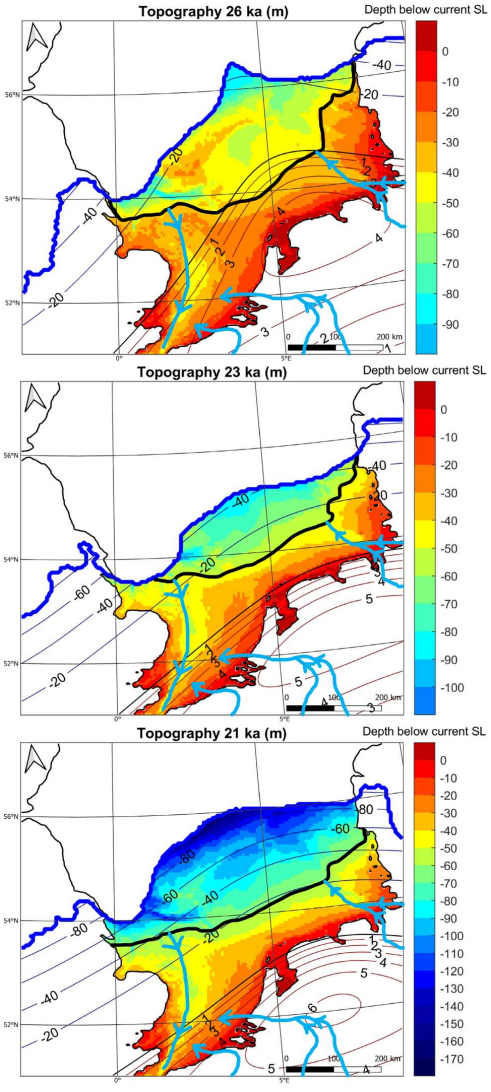

Figure 17: Assumed hydrological situation of the southern North Sea basin A) at 26 ka, B) at 23 ka and C) at 21 ka. Southern proglacial lake limit (bold black line) based on paleotopography (combination of current bathymetry and the GIA resulting from BRITICE-CHRONO, displayed using a 10 m stepwise rainbow colour scale) and on the known existence of Holocene sediments. GIA contours are overlain at 1 m intervals for uplift and at 20 m intervals for depression. Ice margin represented by a bold dark blue line, main river pathways depicted in light blue. Courses of Scheldt river and Meuse and Rhine rivers based on De Clercq et al. (2018) and Busschers et al. (2007) respectively, courses of Weser and Elbe rivers based on the position of the Elbe Paleovalley (Özmaral et al., 2022), southward drainage of the assumed proglacial lake based on paleotopography.

https://doi.org/10.5194/egusphere-2026-6213
Preprint. Discussion started: 26 November 2026
© Author(s) 2026. CC BY 4.0 License.

Busschers et al. (2007) suggested that at the onset of deglaciation, the Rhine flowed close to the zone of maximum forebulge uplift. This is also evident in Fig. 17C, which shows that the most strongly uplifted sections of the Rhine and Meuse occur immediately upstream of their westward deflection. Variations in longitudinal gradient may have influenced incision and aggradation rates independently of sedimentological changes (Busschers et al., 2007). Forebulge-related uplift may therefore also havfe contributed to lateral river migration.

At the end of the last glacial period, the Scheldt shifted from a westward course north of Ghent to a route via Antwerp and further northwestward into the North Sea. This change has commonly been attributed to the formation of the east-west-oriented Maldegem-Stekene coversand ridge (e.g., De Moor and Heyse, 1978), which developed between ~17.5 and 15.5 ka (Derese et al., 2010) and likely blocked the former drainage route through the Scheldt Paleovalley. De Clercq et al. (2018), however, suggested that LGM-related GIA may also have influenced this Lateglacial course change, implying that the coversand ridge was not the only control. According to the GIA model outputs presented here, the forebulge slope in Flanders at the time of the Scheldt diversion was oriented from southwest to northeast. As the Scheldt diverted toward the east and northeast, it therefore followed forebulge isolines or even flowed toward more uplifted areas. Consequently, a direct causal link between GIA-related uplift and the deflection of the Scheldt toward Antwerp cannot be established.

5.4. Further research

In this study, a eustatic (i.e., global) sea-level curve was used to generate paleotopographic maps and estimate paleoshoreline positions. However, because local sea level differs from the eustatic sea level, hydro-isostatic loading was not accounted for. When a high-resolution local sea-level curve for the North Sea basin becomes available –well constrained by sea-level index points tied to specific locations and times– water loading can be incorporated to calculate a more accurate isostatic response. This would improve interpretations, particularly during sea-level highstands. It should be noted, however, that local sea-level curves vary spatially within the North Sea basin. Moreover, not accounting for hydro-isostatic lake loading underestimates basin depth (e.g. Austermann et al., 2022), so the incorporation of water loading could improve the reconstructions of proglacial lake geometries as well.

Hoebe et al. (2024) reconstructed Early Holocene inundation of the southern North Sea basin using local, GIA-modelled sea-level curves and accounting for background basin subsidence. When sufficient data become available for the last glacial period, future studies could similarly employ local rather than eustatic sea-level curves and explicitly include basin subsidence. Improved reconstructions would also benefit from a more complete, high-resolution record of Holocene and older glacial sediment thicknesses across the study area.

Several ice-sheet reconstructions exist for parts of the last glacial cycle. However, there remains a need for well-constrained, high-resolution, and publicly available reconstructions of earlier glaciations that can be used in GIA modelling further back in time. Such reconstructions would help evaluate the role of isostatic adjustment in past river-course changes, including the formation of the Scheldt Paleovalley at the end of

https://doi.org/10.5194/egusphere-2026-6213
Preprint. Discussion started: 26 November 2026
© Author(s) 2026. CC BY 4.0 License.

the penultimate glaciation (De Clercq et al., 2018). Better constraints are also needed on the formation and extent of proglacial lakes during MIS 6 and MIS 12, and on how their drainage may have contributed to breaching and the two-stage opening of the Dover Strait (e.g., Gupta et al., 2017).

Reconstructions of earlier glaciations, and even of older phases of the last glacial period, are increasingly uncertain. Ice-margin data become scarcer with age, as earlier signals are often overprinted or removed during subsequent ice advances and/or marine transgressions. Moreover, translating ice extent into ice thickness remains poorly constrained, as thickness variations are modelled rather than directly observed. Ice-thickness models are typically calibrated using modern ice sheets in Antarctica and Greenland; however, it is unclear whether their dynamics are fully representative of past ice sheets. Despite these uncertainties, this and future studies that better constrain the locations of former proglacial lakes can guide the search for lacustrine sediments in the North Sea basin, which in turn would improve paleotopographic reconstructions.

The choice of Earth parameters is critical in GIA modelling. Although the range of asthenosphere viscosity values commonly used in GIA studies is relatively narrow and produces broadly similar results, lithosphere thickness remains poorly constrained and likely varies significantly between regions due to differences in geological history. Variations in assumed lithosphere thickness can strongly influence model outcomes, underscoring the need for improved constraints on its spatial distribution.

6. CONCLUSIONS

In this study, GIA-related forebulge development and subsidence in the North Sea region were modelled using the PaleoMIST and BRITICE-CHRONO ice-sheet reconstructions. Although PaleoMIST includes the Barents-Kara Ice Sheet, sensitivity tests demonstrate that, for the study area, incorporating the BIIS and the southern FIS is sufficient to produce robust results. In contrast to what was done in some previous GIA studies, both ice sheets must be included to accurately reproduce the regional signal.

The results show that the forebulge migrates spatially through time. Ice-sheet advance displaces the uplift zone away from the centre of ice loading, whereas retreat induces landward migration. Following complete deglaciation of the region of interest, the residual GIA signal no longer migrates laterally but decays monotonically toward zero vertical displacement. During the LGM, maximal forebulge uplift shifted from the northern Netherlands toward the central and southern Netherlands, whereas during less extensive glaciations it was positioned further northwest.

These findings highlight the need for improved empirical constraints on ice limits during earlier phases of the last glacial cycle and preceding glaciations. Although glacial maxima are relatively well constrained, ice limits during less extensive phases remain poorly defined. Because ice-sheet geometry strongly controls lateral mantle flow, uncertainties in ice configuration directly affect GIA predictions, underscoring the importance of accurate reconstructions.

https://doi.org/10.5194/egusphere-2026-6213
Preprint. Discussion started: 26 November 2026
© Author(s) 2026. CC BY 4.0 License.

Improved ice-sheet models must be complemented by refined Earth models. Considerable uncertainty remains regarding appropriate rheological parameter values. Our results demonstrate that Earth structure exerts a first-order control on GIA patterns: lithosphere thickness primarily influences forebulge migration, whereas asthenosphere viscosity strongly affects response magnitude.

GIA substantially influenced the inundation-emersion history of proglacial areas in the North Sea basin. As post-LGM glacio-isostasy continues today, it remains essential for quantifying relative sea-level change and isolating the anthropogenic component of sea-level rise. Despite differences between the two ice-sheet reconstructions –and consequently in simulated GIA and paleotopography– several robust conclusions emerge:

- GIA significantly modified hydrology and drainage patterns in proglacial regions of the central and southern North Sea.
- Forebulge uplift induced river-course adjustments, including southward avulsion of the Rhine during MIS 3.
- GIA-related subsidence increased accommodation space for proglacial lakes near the ice margin, including the proposed southern North Sea lake.

The results provide additional support for the existence of a lake impounded between the ice margin in the north and the forebulge in the southeast, with potential drainage via the Axial Channel toward the Dover Strait and the Atlantic Ocean during MIS 4 and MIS 2. These findings are consistent with evidence for (i) overspill-driven drainage events via the Axial Channel and the Channel River toward the Atlantic Ocean during MIS 2, and (ii) GLOF deposits in the northern North Sea following ice-sheet unzipping and catastrophic lake drainage.

Further GIA modelling is required to test whether similar mechanisms operated during MIS 6 and MIS 12 in relation to the opening of the Dover Strait, and to evaluate the role of glacio-isostasy in earlier river-course reorganisations. In addition, the impact of Quaternary sediment accumulation on paleotopography and the role of hydro-isostasy in driving local relative sea-level change within the North Sea basin warrant further investigation.

CODE AND DATA AVAILABILITY

All scripts used to generate the data depicted in this article will be made publicly available on GitHub upon publication of the manuscript. All data needed to assess the conclusions presented in this article are available within the paper and the supplementary material.

AUTHOR CONTRIBUTION

MDB and RB conceptualised the research. RB designed the methodology, carried out the investigation, visualised and analysed the data and wrote the original draft of the manuscript. MDB supervised the

https://doi.org/10.5194/egusphere-2026-6213
Preprint. Discussion started: 26 November 2026
© Author(s) 2026. CC BY 4.0 License.

research and acquired the funding. RB and MDB validated the results and interpretations and contributed to the review and editing of the manuscript.

COMPETING INTERESTS

The authors declare that they have no conflict of interest.

ACKNOWLEDGEMENTS

This study was carried out in the framework of project RV/21/WALDO ("Where are All the (proglacial) Lake seDiments in the NOrth Sea Basin?") financed by the Belgian Science Policy Office (BELSPO). We would like to thank Philippe Huybrechts (Vrije Universiteit Brussel) and Frank Pattyn (Université libre de Bruxelles) for the essential discussions on the ELRA model. We also thank Sarah Bradley (University of Sheffield), Ruth Plets (Flanders Marine Institute), Morgan Vervoort (Ghent University and Flanders Marine Institute) and Despina Kyriakoudi (Ghent University and Flanders Marine Institute) for the interesting discussions on the results of this study. ChatGPT was used to assist with improving the language, grammar, and readability of the manuscript. The authors reviewed and edited all AI-generated suggestions and take full responsibility for the final content of the manuscript.

7. REFERENCES

Amkreutz, L., Cohen, K., Hijma, M., Odé, O., 2022. Mapping a drowning land, in: Amkreutz, L., van der Vaart-Verschoof, S. (Eds.), Doggerland : Lost World under the North Sea. Sidestone Press, pp. 37–41.

Argus, D.F., Peltier, W.R., Drummond, R., Moore, A.W., 2014. The Antarctica component of postglacial rebound model ICE-6G_C (VM5a) based on GPS positioning, exposure age dating of ice thicknesses, and relative sea level histories. Geophys J Int 198, 537–563. https://doi.org/10.1093/GJI/GGU140

Austermann, J., Wickert, A.D., Pico, T., Kingslake, J., Callaghan, K.L., Creel, R.C., 2022. Glacial isostatic adjustment shapes proglacial lakes over glacial cycles. Geoph Res Lett 49, e2022GL101191. https://doi.org/10.1029/2022GL101191

Balson, P.S. (comp.), 1988. East Anglia sheet - Sea Bed Sediments. Geological Survey 1:250000 Series, BGS.

Balson, P.S., D'Olier, B. (comps.), 1990. Thames Estuary sheet - Sea Bed Sediments and Quaternary Geology. Geological Survey 1:250000 Series, BGS.

Balson, P.S., Laban, C., Schüttenhelm, R.T.E., Paepe, R., Baeteman, C. (comps.), 1991. Ostend sheet - Sea Bed Sediments and Holocene Geology. Geological Survey 1:250000 Series, BGS, RGD & BGD.

Batchelor, C. L., Margold, M., Krapp, M., Murton, D. K., Dalton, A. S., Gibbard, P. L., Stokes, C. R., Murton, J. B., Manica, A., 2019. The configuration of Northern Hemisphere ice sheets through the Quaternary. Nat Commun 10, 1–10. https://doi.org/10.1038/s41467-019-11601-2

Bergstrand, S., Scherneck, H.G., Milne, G.A., Johansson, J.M., 2005. Upper mantle viscosity from continuous GPS baselines in Fennoscandia. J Geodyn 39, 91–109. https://doi.org/10.1016/J.JOG.2004.08.004

https://doi.org/10.5194/egusphere-2026-6213
Preprint. Discussion started: 26 November 2026
© Author(s) 2026. CC BY 4.0 License.

Bigg, G.R., Clark, C.D., Greenwood, S.L., Haflidason, H., Hughes, A.L.C., Levine, R.C., Nygård, A., Sejrup, H.P., 2012. Sensitivity of the North Atlantic circulation to break-up of the marine sectors of the NW European ice sheets during the last Glacial: A synthesis of modelling and palaeoceanography. Glob Planet Change 98–99, 153–165. https://doi.org/10.1016/J.GLOPLACHA.2012.09.004

Bradley, S.L., Milne, G.A., Shennan, I., Edwards, R., 2011. An improved glacial isostatic adjustment model for the British Isles. J Quat Sci 26, 541–552. https://doi.org/10.1002/jqs.1481

Brotchie, J.F., Silvester, R., 1969. On crustal flexure. J Geophys Res 74, 5240–5252. https://doi.org/10.1029/JB074I022P05240

Bueler, E., Brown, J., 2009. Shallow shelf approximation as a "sliding law" in a thermomechanically coupled ice sheet model. J Geophys Res 114. https://doi.org/10.1029/2008JF001179

Busschers, F.S., Kasse, C., van Balen, R.T., Vandenberghe, J., Cohen, K.M., Weerts, H.J.T., Wallinga, J., Johns, C., Cleveringa, P., Bunnik, F.P.M., 2007. Late Pleistocene evolution of the Rhine-Meuse system in the southern North Sea basin: imprints of climate change, sea-level oscillation and glacio-isostacy. Quat Sci Rev 26, 3216–3248. https://doi.org/10.1016/j.quascirev.2007.07.013

Cameron, T.D.J., Crosby, A., Balson, P.S., Jeffery, D.H., Lott, G.K., Bulat, J., Harrison, D.J., 1992. United Kingdom offshore regional report: The geology of the southern North Sea. HMSO for the British Geological Survey, London.

Cameron, T.D.J., Laban, C., Schüttenhelm, R.T.E. (comps.), 1984. Flemish Bight sheet - Sea Bed Sediments and Holocene Geology. Geological Survey 1:250000 Series, BGS & RGD.

Carr, S.J., Holmes, R., van der Meer, J.J.M., Rose, J., 2006. The Last Glacial Maximum in the North Sea Basin: micromorphological evidence of extensive glaciation. J Quat Sci 21, 131–153. https://doi.org/10.1002/JQS.950

Clark, C.D., Ely, J.C., Fabel, D., Bradley, S.L., 2022a. BRITICE-CHRONO maps and GIS data of the last British-Irish Ice Sheet 31 to 15 ka, including model reconstruction, geochronometric age spreadsheet, palaeotopographies and coastline positions. https://doi.org/10.1594/PANGAEA.945729

Clark, C.D., Ely, J.C., Hindmarsh, R.C.A., Bradley, S., Ignéczi, A., Fabel, D., Ó Cofaigh, C., Chiverrell, R.C., Scourse, J., Benetti, S., Bradwell, T., Evans, D.J.A., Roberts, D.H., Burke, M., Callard, S.L., Medialdea, A., Saher, M., Small, D., Smedley, R.K., Gasson, E., Gregoire, L., Gandy, N., Hughes, A.L.C., Ballantyne, C., Bateman, M.D., Bigg, G.R., Doole, J., Dove, D., Duller, G.A.T., Jenkins, G.T.H., Livingstone, S.L., McCarron, S., Moreton, S., Pollard, D., Praeg, D., Sejrup, H.P., Van Landeghem, K.J.J., Wilson, P., 2022b. Growth and retreat of the last British–Irish Ice Sheet, 31 000 to 15 000 years ago: the BRITICE-CHRONO reconstruction. Boreas 51, 699–758. https://doi.org/10.1111/BOR.12594

Clark, P.U., Mix, A.C., 2002. Ice sheets and sea level of the Last Glacial Maximum. Quat Sci Rev 21, 1–7. https://doi.org/10.1016/S0277-3791(01)00118-4

Clarke, G.K.C., Mathews, W.H., Pack, R.T., 1984. Outburst Floods from Glacial Lake Missoula. Quat Res 22, 289–299. https://doi.org/10.1016/0033-5894(84)90023-1

Cohen, K.M., Gibbard, P.L., Weerts, H.J.T., 2014. North Sea palaeogeographical reconstructions for the last 1 Ma. Netherlands Journal of Geosciences 93, 7–29. https://doi.org/10.1017/NJG.2014.12

Cohen, K.M., Westley, K., Erkens, G., Hijma, M.P., Weerts, H.J.T., 2017. The North Sea, in: Flemming, N.C., Harff, J., Moura, D., Burgess, A., Bailey, G.N. (Eds.), Submerged Landscapes of the European Continental

https://doi.org/10.5194/egusphere-2026-6213
Preprint. Discussion started: 26 November 2026
© Author(s) 2026. CC BY 4.0 License.

Shelf: Quaternary Paleoenvironments. Wiley Blackwell, pp. 147–186. https://doi.org/10.1002/9781118927823.CH7

Collier, J.S., Oggioni, F., Gupta, S., Garcia-Moreno, D., Trentesaux, A., De Batist, M., 2015. Streamlined islands and the English Channel megaflood hypothesis. Glob. Planet. Change 135, 190-206. https://doi.org/10.1016/j.gloplacha.2015.11.004

Cotterill, C.J., Phillips, E., James, L., Forsberg, C.F., Tjelta, T.I., Carter, G., Dove, D., 2017. The evolution of the Dogger Bank, North Sea: A complex history of terrestrial, glacial and marine environmental change. Quat Sci Rev 171, 136–153. https://doi.org/10.1016/J.QUASCIREV.2017.07.006

Coulon, V., Bulthuis, K., Whitehouse, P.L., Sun, S., Haubner, K., Zipf, L., Pattyn, F., 2021. Contrasting Response of West and East Antarctic Ice Sheets to Glacial Isostatic Adjustment. J Geophys Res Earth Surf 126, e2020JF006003. https://doi.org/10.1029/2020JF006003

de Boer, B., van de Wal, R., 2021. Ice Sheets in the Cenozoic, in: Fowler Andrew and Ng, F. (Ed.), Glaciers and Ice Sheets in the Climate System: The Karthaus Summer School Lecture Notes. Springer International Publishing, Cham, pp. 415–430. https://doi.org/10.1007/978-3-030-42584-5_16

De Clercq, M., 2018. Drowned landscapes of the Belgian Continental Shelf: implications for northwest European landscape evolution and preservation potential for submerged heritage (PhD thesis). Ghent University, Belgium.

De Clercq, M., Missiaen, T., Wallinga, J., Zurita Hurtado, O., Versendaal, A., Mathys, M., De Batist, M., 2018. A well-preserved Eemian incised-valley fill in the southern North Sea Basin, Belgian Continental Shelf - Coastal Plain: Implications for northwest European landscape evolution. Earth Surf Process Landf 43, 1913–1942. https://doi.org/10.1002/ESP.4365

De Moor, G., Heyse, I., 1978. De morfologische evolutie van de Vlaamse Vallei. De aardrijkskunde 4, 343–375.

Derese, C., Vandenberghe, D.A.G., Zwertvaegher, A., Court-Picon, M., Crombé, P., Verniers, J., Van Den Haute, P., 2010. The timing of aeolian events near archaeological settlements around Heidebos (Moervaart area, N Belgium). Netherlands Journal of Geosciences 89, 173–186. https://doi.org/10.1017/S0016774600000688

Eaton, S.J., Hodgson, D.M., Barlow, N.L.M., Mortimer, E.E.J., Mellett, C.L., 2020. Palaeogeographical changes in response to glacial–interglacial cycles, as recorded in Middle and Late Pleistocene seismic stratigraphy, southern North Sea. J Quat Sci 35, 760–775. https://doi.org/10.1002/JQS.3230

Ehlers, J., Gibbard, P.L., Hughes, P.D., 2018. Quaternary Glaciations and Chronology, in: Menzies, J., van der Meer, J.J.M. (Eds.), Past Glacial Environments: Second Edition. Elsevier, pp. 77–101. https://doi.org/10.1016/B978-0-08-100524-8.00003-8

Emery, A.R., Hodgson, D.M., Barlow, N.L.M., Carrivick, J.L., Cotterill, C.J., Phillips, E., 2019. Left High and Dry: Deglaciation of Dogger Bank, North Sea, Recorded in Proglacial Lake Evolution. Front Earth Sci 7, 476415. https://doi.org/10.3389/FEART.2019.00234

Farrell, W.E., Clark, J.A., 1976. On Postglacial Sea Level. Geophys J Int 46, 647–667. https://doi.org/10.1111/J.1365-246X.1976.TB01252.X

Figge, K., 1980. Das Elbe—Urstromtal im Bereich der Deutschen Bucht (Nordsee). E&G – Quaternary Science Journal 30, 203–212. https://doi.org/10.23689/FIDGEO-911

https://doi.org/10.5194/egusphere-2026-6213
Preprint. Discussion started: 26 November 2026
© Author(s) 2026. CC BY 4.0 License.

Fjeldskaar, W., 1994. The amplitude and decay of the glacial forebulge in Fennoscandia. Norsk Geologisk Tidsskrift 74, 2–8.

García-Moreno, D., 2017. Origin and geomorphology of the Dover Strait and southern North Sea palaeovalleys and palaeo-depressions.

Gibbard, P., 2007. Europe cut adrift. Nature 448, 259–260. https://doi.org/10.1038/448259a

Gibbard, P.L., 1995. The formation of the Strait of Dover. Geol Soc Spec Publ 96, 15–26. https://doi.org/10.1144/GSL.SP.1995.096.01.03

Gibbard, P.L., Cohen, K.M., 2015. Quaternary evolution of the North Sea and the English Channel. Proceedings of the Open University Geological Society 1, 63–74.

Gowan, E.J., 2019. Global ice sheet reconstruction for the past 80000 years. https://doi.org/10.1594/PANGAEA.905800

Gowan, E.J., Tregoning, P., Purcell, A., Lea, J., Fransner, O.J., Noormets, R., Dowdeswell, J.A., 2016. ICESHEET 1.0: A program to produce paleo-ice sheet reconstructions with minimal assumptions. Geosci Model Dev 9, 1673–1682. https://doi.org/10.5194/GMD-9-1673-2016

Gowan, E.J., Zhang, X., Khosravi, S., Rovere, A., Stocchi, P., Hughes, A.L.C., Gyllencreutz, R., Mangerud, J., Svendsen, J.I., Lohmann, G., 2021. A new global ice sheet reconstruction for the past 80 000 years. Nat Commun 12, 1–9. https://doi.org/10.1038/s41467-021-21469-w

Graham, A.G.C., Stoker, M.S., Lonergan, L., Bradwell, T., Stewart, M.A., 2011. The Pleistocene glaciations of the North Sea basin, Developments in Quaternary Science. https://doi.org/10.1016/B978-0-444-53447-7.00021-0

Greve, R., 2001. Glacial Isostasy: Models for the Response of the Earth to Varying Ice Loads, in: Straughan, B., Greve, R., Ehrentraut, H., Wang, Y. (Eds.), Continuum Mechanics and Applications in Geophysics and the Environment. Springer, Berlin, Heidelberg, pp. 307–325. https://doi.org/10.1007/978-3-662-04439-1_16

Gupta, S., Collier, J.S., Garcia-Moreno, D., Oggioni, F., Trentesaux, A., Vanneste, K., De Batist, M., Camelbeeck, T., Potter, G., Van Vliet-Lanoë, B., Arthur, J.C.R., 2017. Two-stage opening of the Dover Strait and the origin of island Britain. Nat Commun 8, 1–12. https://doi.org/10.1038/ncomms15101

Gupta, S., Collier, J.S., Palmer-Felgate, A., Potter, G., 2007. Catastrophic flooding origin of shelf valley systems in the English Channel. Nature 448, 342–345. https://doi.org/10.1038/nature06018

Harrison, D.J., Laban, C., Schüttenhelm, R.T.E. (comps.), 1987. Indefatigable sheet - Sea Bed Sediments and Holocene Geology. Geological Survey 1:250000 Series, BGS & RGD.

Helmens, K.F., 2014. The Last Interglacial–Glacial cycle (MIS 5–2) re-examined based on long proxy records from central and northern Europe. Quat Sci Rev 86, 115–143. https://doi.org/10.1016/J.QUASCIREV.2013.12.012

Hijma, M.P., Cohen, K.M., Roebroeks, W., Westerhoff, W.E., Busschers, F.S., 2012. Pleistocene Rhine-Thames landscapes - a geological background for hominin occupation patterns in the southern North Sea. J Quat Sci 27, 17–39. https://doi.org/10.1016/J.QUAINT.2012.08.362

Hjelstuen, B.O., Sejrup, H.P., Valvik, E., Becker, L.W.M., 2018. Evidence of an ice-dammed lake outburst in the North Sea during the last deglaciation. Mar Geol 402, 118–130. https://doi.org/10.1016/J.MARGEO.2017.11.021

https://doi.org/10.5194/egusphere-2026-6213
Preprint. Discussion started: 26 November 2026
© Author(s) 2026. CC BY 4.0 License.

Hoebe, P.W., Cohen, K.M., Busschers, F.S., van Heteren, S., Peeters, J.H.M., 2024. Early Holocene inundation of Doggerland and its impact on hunter-gatherers: An inundation model and dates-as-data approach. Quaternary International 694, 26–50. https://doi.org/10.1016/J.QUAINT.2024.05.006

Houmark-Nielsen, M., Kjær, K.H., 2003. Southwest Scandinavia, 40–15 kyr BP: palaeogeography and environmental change. J Quat Sci 18, 769–786. https://doi.org/10.1002/JQS.802

Hughes, A.L.C., Gyllencreutz, R., Lohne, Ø.S., Mangerud, J., Svendsen, J.I., 2016. The last Eurasian ice sheets – a chronological database and time-slice reconstruction, DATED-1. Boreas 45, 1–45. https://doi.org/10.1111/BOR.12142

Hughes, P.D., Gibbard, P.L., Ehlers, J., 2013. Timing of glaciation during the last glacial cycle: evaluating the concept of a global 'Last Glacial Maximum' (LGM). Earth Sci Rev 125, 171–198. https://doi.org/10.1016/J.EARSCIREV.2013.07.003

Huybrechts, P., de Wolde, J., 1999. The Dynamic Response of the Greenland and Antarctic Ice Sheets to Multiple-Century Climatic Warming. J Clim 12, 2169–2188. https://doi.org/10.1175/1520-0442(1999)012<2169:TDROTG>2.0.CO;2

Ingólfsson, Ó., Landvik, J.Y., 2013. The Svalbard–Barents Sea ice-sheet – Historical, current and future perspectives. Quat Sci Rev 64, 33–60. https://doi.org/10.1016/J.QUASCIREV.2012.11.034

Jeffery, D., Graham, C., Wright, S., Laban, C., Schüttenhelm, R.T.E. (comps.), 1990. Dogger sheet - Sea Bed Sediments and Holocene Geology. Geological Survey 1:250000 Series, BGS & RGD.

Jeffery, D., Laban, C., Niessen, A.C.H.M., Schüttenhelm, R.T.E. (comps.), 1988. Silver Well sheet - Sea Bed Sediments and Holocene Geology. Geological Survey 1:250000 Series, BGS & RGD.

Kiden, P., Denys, L., Johnston, P., 2002. Late Quaternary sea-level change and isostatic and tectonic land movements along the Belgian-Dutch North Sea coasts: Geological data and model results. J Quat Sci 17, 535–546. https://doi.org/10.1002/jqs.709

Kyriakoudi, D., De Batist, M., Vervoort, M., Mestdagh, T., Missiaen, T., Grant, M., Hill, T., Kinnaird, T., Plets, R., 2026. Evidence of a Weichselian MIS 3 proglacial lake south of Dogger Bank (southern North Sea). Quat Sci Rev 390, 110190. https://doi.org/10.1016/J.QUASCIREV.2026.110190

Lambeck, K., 1995. Late Devensian and Holocene shorelines of the British Isles and North Sea from models of glacio-hydro-isostatic rebound. J Geol Soc London 152, 437–448. https://doi.org/10.1144/gsjgs.152.3.0437

Lambeck, K., Esat, T.M., Potter, E.K., 2002. Links between climate and sea levels for the past three million years. Nature 419, 199–206. https://doi.org/10.1038/nature01089

Lambeck, K., Purcell, A., Funder, S., Kjær, K., Larsen, E., Möller, P., 2006. Constraints on the Late Saalian to early Middle Weichselian ice sheet of Eurasia from field data and rebound modelling. Boreas 35, 539–575. https://doi.org/10.1080/03009480600781875

Lambeck, K., Rouby, H., Purcell, A., Sun, Y., Sambridge, M., 2014. Sea level and global ice volumes from the Last Glacial Maximum to the Holocene. Proc Natl Acad Sci USA 111, 15296–15303. https://doi.org/10.1073/PNAS.1411762111

Le Meur, E., 1996. Isostatic postglacial rebound over Fennoscandia with a self-gravitating spherical visco-elastic Earth model. Ann Glaciol 23, 318–327. https://doi.org/10.3189/S0260305500013598

https://doi.org/10.5194/egusphere-2026-6213
Preprint. Discussion started: 26 November 2026
© Author(s) 2026. CC BY 4.0 License.

Le Meur, E., Huybrechts, P., 1996. A comparison of different ways of dealing with isostasy: examples from modelling the Antarctic ice sheet during the last glacial cycle. Ann Glaciol 23, 309–317. https://doi.org/10.3189/S0260305500013586

Lekens, W.A.H., Sejrup, H.P., Haflidason, H., Knies, J., Richter, T., 2006. Meltwater and ice rafting in the southern Norwegian Sea between 20 and 40 calendar kyr B.P.: Implications for Fennoscandian Heinrich events. Paleoceanography 21, PA3013. https://doi.org/10.1029/2005PA001228

Lidberg, M., Johansson, J.M., Scherneck, H.G., Milne, G.A., 2010. Recent results based on continuous GPS observations of the GIA process in Fennoscandia from BIFROST. J Geodyn 50, 8–18. https://doi.org/10.1016/J.JOG.2009.11.010

Ménot, G., Bard, E., Rostek, F., Weijers, J.W.H., Hopmans, E.C., Schouten, S., Sinninghe Damsté, J.S., 2006. Early reactivation of European rivers during the last deglaciation. Science (1979) 313, 1623–1625. https://doi.org/10.1126/SCIENCE.1130511

Milne, G.A., Mitrovica, J.X., 1998. Postglacial sea-level change on a rotating Earth. Geophys J Int 133, 1–19. https://doi.org/10.1046/J.1365-246X.1998.1331455.X

Milne, G.A., Shennan, I., Youngs, B.A.R., Waugh, A.I., Teferle, F.N., Bingley, R.M., Bassett, S.E., Cuthbert-Brown, C., Bradley, S.L., 2006. Modelling the glacial isostatic adjustment of the UK region. Philosophical Transactions of the Royal Society A: Mathematical, Physical and Engineering Sciences 364, 931–948. https://doi.org/10.1098/rsta.2006.1747

Mörner, N.A., 1979. The Fennoscandian uplift and late cenozoic geodynamics: geological evidence. GeoJournal 3, 287–318. https://doi.org/10.1007/BF00177634

Murton, D.K., Murton, J.B., 2012. Middle and Late Pleistocene glacial lakes of lowland Britain and the southern North Sea Basin. Quat Int 260, 115–142. https://doi.org/10.1016/J.QUAINT.2011.07.034

Näslund, J.-O., 2010. Ice sheet dynamics, in: Climate and Climate-Related Issues for the Safety Assessment SR-Site, Technical Report TR-10-49. Swedish Nuclear Fuel and Waste Management Co. (SKB), Stockholm, Sweden.

O'Connor, J.E., Baker, V.R., 1992. Magnitudes and implications of peak discharges from glacial Lake Missoula. GSA Bulletin 104, 267–279. https://doi.org/10.1130/0016-7606(1992)104<0267:MAIOPD>2.3.CO;2

Oldham, K.B., Myland, J.C., Spanier, J., 2008. The Kelvin Functions, in: An Atlas of Functions. Springer, New York, NY, pp. 577–584. https://doi.org/10.1007/978-0-387-48807-3_56

Özmaral, A., Abegunrin, A., Keil, H., Hepp, D.A., Schwenk, T., Lantzsch, H., Mörz, T., Spiess, V., 2022. The Elbe Palaeovalley: Evolution from an ice-marginal valley to a sedimentary trap (SE North Sea). Quat Sci Rev 282, 107453. https://doi.org/10.1016/J.QUASCIREV.2022.107453

Papenmeier, S., Hass, H.C., 2020. Revisiting the Paleo Elbe Valley: Reconstruction of the Holocene, Sedimentary Development on Basis of High-Resolution Grain Size Data and Shallow Seismics. Geosciences (Basel) 10, 505. https://doi.org/10.3390/geosciences10120505

Patton, H., Hubbard, A., Andreassen, K., Auriac, A., Whitehouse, P.L., Stroeven, A.P., Shackleton, C., Winsborrow, M., Heyman, J., Hall, A.M., 2017. Deglaciation of the Eurasian ice sheet complex. Quat Sci Rev 169, 148–172. https://doi.org/10.1016/j.quascirev.2017.05.019

https://doi.org/10.5194/egusphere-2026-6213
Preprint. Discussion started: 26 November 2026
© Author(s) 2026. CC BY 4.0 License.

Patton, H., Hubbard, A., Andreassen, K., Winsborrow, M., Stroeven, A.P., 2016. The build-up, configuration, and dynamical sensitivity of the Eurasian ice-sheet complex to Late Weichselian climatic and oceanic forcing. Quat Sci Rev 153, 97–121. https://doi.org/10.1016/J.QUASCIREV.2016.10.009

Pattyn, F., 2017. Sea-level response to melting of Antarctic ice shelves on multi-centennial timescales with the fast Elementary Thermomechanical Ice Sheet model (f.ETISh v1.0). Cryosphere 11, 1851–1878. https://doi.org/10.5194/TC-11-1851-2017

Peltier, W.R., 2004. Global glacial isostasy and the surface of the ice-age earth: The ICE-5G (VM2) model and GRACE. Annu Rev Earth Planet Sci 32, 111–149. https://doi.org/10.1146/ANNUREV.EARTH.32.082503.144359

Peltier, W.R., Argus, D.F., Drummond, R., 2015. Space geodesy constrains ice age terminal deglaciation: The global ICE-6G_C (VM5a) model. J Geophys Res Solid Earth 120, 450–487. https://doi.org/10.1002/2014JB011176

Roberts, D.H., Evans, D.J.A., Callard, S.L., Clark, C.D., Bateman, M.D., Medialdea, A., Dove, D., Cotterill, C.J., Saher, M., Cofaigh, C., Chiverrell, R.C., Moreton, S.G., Fabel, D., Bradwell, T., 2018. Ice marginal dynamics of the last British-Irish Ice Sheet in the southern North Sea: Ice limits, timing and the influence of the Dogger Bank. Quat Sci Rev 198, 181–207. https://doi.org/10.1016/J.QUASCIREV.2018.08.010

Schumacher, M., King, M.A., Rougier, J., Sha, Z., Khan, S.A., Bamber, J.L., 2018. A new global GPS data set for testing and improving modelled GIA uplift rates. Geophys J Int 214, 2164–2176. https://doi.org/10.1093/GJI/GGY235

Sejrup, H.P., Clark, C.D., Hjelstuen, B.O., 2016. Rapid ice sheet retreat triggered by ice stream debuttressing: Evidence from the North Sea. Geology 44, 355–358. https://doi.org/10.1130/G37652.1

Spada, G., Stocchi, P., 2007. SELEN: A Fortran 90 program for solving the "sea-level equation." Comput Geosci 33, 538–562. https://doi.org/10.1016/J.CAGEO.2006.08.006

Steffen, H., 2006. Determination of a consistent viscosity distribution in the Earth's mantle beneath northern and Central Europe. Institut für Geologische Wissenschaften der Freie Universität Berlin. https://doi.org/10.23689/fidgeo-339

Steffen, H., Wu, P., 2011. Glacial isostatic adjustment in Fennoscandia-A review of data and modeling. J Geodyn. https://doi.org/10.1016/j.jog.2011.03.002

Svendsen, J.I., Alexanderson, H., Astakhov, V.I., Demidov, I., Dowdeswell, J.A., Funder, S., Gataullin, V., Henriksen, M., Hjort, C., Houmark-Nielsen, M., Hubberten, H.W., Ingólfsson, Ó., Jakobsson, M., Kjær, K.H., Larsen, E., Lokrantz, H., Lunkka, J.P., Lyså, A., Mangerud, J., Matiouchkov, A., Murray, A., Möller, P., Niessen, F., Nikolskaya, O., Polyak, L., Saarnisto, M., Siegert, C., Siegert, M.J., Spielhagen, R.F., Stein, R., 2004. Late Quaternary ice sheet history of northern Eurasia. Quat Sci Rev 23, 1229–1271. https://doi.org/10.1016/J.QUASCIREV.2003.12.008

Tesauro, M., Audet, P., Kaban, M.K., Cloetingh, S., 2012. The effective elastic thickness of the continental lithosphere: Comparison between rheological and inverse approaches. Geochemistry, Geophysics, Geosystems 13. https://doi.org/10.1029/2012GC004162

The MathWorks Inc., 2022. MATLAB version: 9.13.0 (R2022b).

Toucanne, S., Soulet, G., Freslon, N., Silva Jacinto, R., Dennielou, B., Zaragosi, S., Eynaud, F., Bourillet, J.-F., Bayon, G., 2015. Millennial-scale fluctuations of the European Ice Sheet at the end of the last glacial,

https://doi.org/10.5194/egusphere-2026-6213
Preprint. Discussion started: 26 November 2026
© Author(s) 2026. CC BY 4.0 License.

and their potential impact on global climate. Quat Sci Rev 123, 113–133. https://doi.org/10.1016/J.QUASCIREV.2015.06.010

Toucanne, S., Zaragosi, S., Bourillet, J.-F., Marieu, V., Cremer, M., Kageyama, M., Van Vliet-Lanoë, B., Eynaud, F., Turon, J.-L., Gibbard, P.L., 2010. The first estimation of Fleuve Manche palaeoriver discharge during the last deglaciation: Evidence for Fennoscandian ice sheet meltwater flow in the English Channel ca 20–18 ka ago. Earth Planet Sci Lett 290, 459–473. https://doi.org/10.1016/J.EPSL.2009.12.050

Vervoort, M., Plets, R., Kyriakoudi, D., Mestdagh, T., Waajen-Labee, I., Wesselingh, F., Grant, M., Kinnaird, T., Missiaen, T., De Batist, M., (submitted). New chronostratigraphic insights into the evolution of the Axial Channel (southern North Sea) from preserved Upper Pleistocene deposits. Quat Sci Rev.

Vink, A., Steffen, H., Reinhardt, L., Kaufmann, G., 2007. Holocene relative sea-level change, isostatic subsidence and the radial viscosity structure of the mantle of northwest Europe (Belgium, the Netherlands, Germany, southern North Sea). Quat Sci Rev 26, 3249–3275. https://doi.org/10.1016/j.quascirev.2007.07.014

Westaway, R., Bridgland, D.R., 2010. Causes, consequences and chronology of large-magnitude palaeoflows in Middle and Late Pleistocene river systems of northwest Europe. Earth Surf Process Landf 35, 1071–1094. https://doi.org/10.1002/ESP.1968

Westaway, R., Bridgland, D., White, M., 2006. The Quaternary uplift history of central southern England: evidence from the terraces of the Solent River system and nearby raised beaches. Quat Sci Rev 25, 2212–2250. https://doi.org/10.1016/j.quascirev.2005.06.005

Whitehouse, P.L., 2018. Glacial isostatic adjustment modelling: Historical perspectives, recent advances, and future directions. Earth Surface Dynamics 6, 401–429. https://doi.org/10.5194/ESURF-6-401-2018

Winkelmann, R., Martin, M.A., Haseloff, M., Albrecht, T., Bueler, E., Khroulev, C., Levermann, A., 2011. The Potsdam Parallel Ice Sheet Model (PISM-PIK) - Part 1: Model description. Cryosphere 5, 715–726. https://doi.org/10.5194/TC-5-715-2011